PHYSICAL REVIEW C **76**, 014602 (2007)

Interaction of two deformed, arbitrarily oriented nuclei

V. Yu. Denisov and N. A. Pilipenko
Institute for Nuclear Research, Prospect Nauki 47, 03680 Kiev, Ukraine
(Received 19 January 2007; published 6 July 2007)

A simple expression for the Coulomb interaction of two deformed, arbitrarily oriented, axially symmetric nuclei is obtained. An accurate approximation for the nuclear part of the interaction between these nuclei has been proposed. The properties of the total potentials between nuclei with prolate-prolate, prolate-oblate, and oblate-oblate deformations at various orientations are discussed. The particularities of the total potentials for the systems leading to superheavy elements are considered in detail. The influence of quadrupole and hexadecapole deformations of both nuclei at various orientations on the barrier height and potential pocket properties is studied.

DOI: 10.1103/PhysRevC.76.014602 PACS number(s): 25.60.Pj, 25.70.Gh, 25.70.Jj

I. INTRODUCTION

The ground state of nuclei is characterized by shape, which can be spherical or deformed. Nuclei of various shapes have been used in collision experiments. The shapes of colliding nuclei are very important for the barrier height and other properties of a nuclear reaction. It has been shown both experimentally and theoretically that the subbarrier fusion of spherical and well-deformed nuclei in the ground state is strongly enhanced by deformation [1–6]. The height of the barrier is especially important for the production of heavy and superheavy elements (SHE). Nuclear reactions involving two deformed nuclei have been used in various laboratories for SHE production [7–19]. The radiochemistry of SHE is done often in reactions between deformed actinide targets and well-deformed light projectiles [11,14,16,18,20]. Subbarrier fusion reactions between well-deformed isotopes of F, Ne, and Mg are very important in the burning of stars [21–23], because these reactions determine the evolution of stars and the parameters of the equilibrium state of hot stellar matter. Therefore it is very important to study properties of the interaction potential between two deformed, arbitrarily oriented nuclei.

The interaction potential between nuclei consists of nuclear, Coulomb, and centrifugal parts. The Coulomb part is related to a six-dimensional integral [24–31]. The nuclear part of a nucleus-nucleus potential is given by six- or three-dimensional integrals in the framework of various models [24,26–28,30–34]. The evaluation of these integrals is an intricate numerical problem, especially when the ground states of interacting nuclei are well deformed. Because of this, it is very desirable to have a simple, accurate approach for evaluating the nucleus-nucleus potential between deformed, arbitrarily oriented nuclei.

The Coulomb interaction of two deformed nuclei is often approximated by various expressions of different accuracy [2,4–6,35]. As a rule, the first-order (linear) corrections to the Coulomb interaction of two point nuclei are taken into account [4,6,35]. Some terms of the second-order corrections for the specific orientation of two deformed nuclei are given in Ref. [2]. Below we derive an expression containing all linear and second-order corrections on quadrupole deformation for the Coulomb interaction of two arbitrarily oriented, axially symmetric nuclei.

The expression for the nuclear part of the interaction between two spherical nuclei is obtained by using the semimicroscopic approximation in Ref. [26]. This expression is derived by fitting the potentials evaluated for various nucleus-nucleus systems. The heights and radii of the experimental fusion barriers are well described by this potential [26,36,37]. Using both the proximity theorem [38] and the expression for potential from Ref. [26], we obtain below a simple approach for the nuclear part of the interaction between two deformed, arbitrarily oriented nuclei. Note that the values of potential evaluated by applying the proximity theorem and the double-folding method agree fairly well [32,33]. The proximity theorem is often applied to the evaluation of the nuclear part of the potential between deformed nuclei [32,33,39]. However, our approach to the nuclear part of the potential takes into account all linear and second-order terms of the quadrupole deformation parameters of both nuclei.

There are many interesting features in the interaction between spherical and well-deformed nuclei [27–29,39]. These peculiarities are especially important in the synthesis of SHE. Some specific properties of reactions between two deformed nuclei are also discussed in Refs. [28,32–34,39,40]. Below we analyze in detail the dependence of the nucleus-nucleus potential on various orientations of deformed nuclei in the framework of our approach. We discuss peculiarities of the potential between two well-deformed nuclei. The potentials for various systems leading to the SHE are studied. The interplay between the features of the potential and the formation of a very heavy compound nucleus is also considered in detail. Some results of this paper have been presented very briefly in Ref. [41].

The expression for the Coulomb interaction between two arbitrary oriented axially symmetric deformed nuclei is obtained in Sec. II. Our approximation for the evaluation of the nuclear part of the nucleus-nucleus potential is discussed in Sec. III. Sec. IV is devoted to the detailed consideration of various features of the nucleus-nucleus interaction for arbitrarily oriented deformed nuclei. Our conclusion is given in Sec. V.

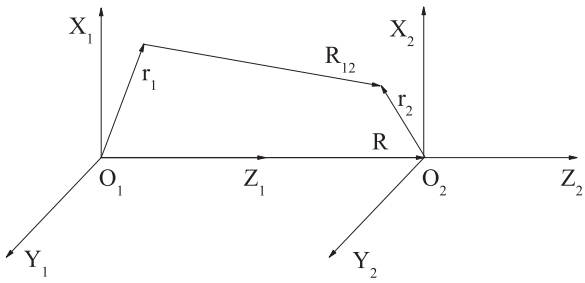

FIG. 1. Coordinate systems related to the mass centers of corresponding nuclei.

II. THE COULOMB INTERACTION OF TWO AXIALLY SYMMETRIC NUCLEI

The Coulomb interaction of two nuclei at distances between their mass centers R is

$$V_C(R) = e^2 \int \frac{\rho_1(\mathbf{r}_1)\rho_2(\mathbf{r}_2)}{|\mathbf{R}+\mathbf{r}_2-\mathbf{r}_1|} d\mathbf{r}_1 d\mathbf{r}_2, \tag{1}$$

where e is the proton charge, and $\rho_i(\mathbf{r}_i)$ is the proton density in the nucleus $i, i = 1, 2$. The vectors $\mathbf{r}_i$ are determined in the coordinate systems O_1 and O_2 as illustrated in Fig. 1. The origins of these coordinate systems are connected to the mass centers of the corresponding nuclei.

The denominator in Eq. (1) can be presented using different expressions [42,43], but the most useful expression for our purpose is (see Ref. [43])

$$\frac{1}{|\mathbf{R}+\mathbf{r}_2-\mathbf{r}_1|} = \sum_{\ell_1,\ell_2=0}^{\infty} \frac{r_1^{\ell_1} r_2^{\ell_2}}{R^{\ell_1+\ell_2+1}} \frac{4\pi(-1)^{\ell_2}(\ell_1+\ell_2)!}{\sqrt{(2\ell_1+1)(2\ell_2+1)}} \times \sum_m \frac{Y_{\ell_1 m}(\vartheta_1,\varphi_1) Y_{\ell_2 -m}(\vartheta_2,\varphi_2)}{\sqrt{(\ell_1+m)!(\ell_1-m)!(\ell_2+m)!(\ell_2-m)!}}, \tag{2}$$

where $Y_{\ell m}(\vartheta,\varphi)$ is the spherical harmonic functions [42], and $r_i, \vartheta_i, \varphi_i$ are the spherical coordinates in the laboratory coordinate system O_i. Note that $Y_{\ell m}(\vartheta,\varphi)$ vanish when $|m| > \ell$.

We consider the interaction of two arbitrarily oriented, axially symmetric nuclei. The mutual orientation of axially symmetric nuclei can be specified by the angles between the axial-symmetry axes of corresponding nuclei and axes O_1Z_1 or O_2Z_2. We choose the directions of coordinates X_1 and Y_1 in such a way that an axial-symmetry axis of the first nucleus is located in the plane X_1Z_1 without the loss of generality. Θ_1 is the angle between the axial-symmetry axis of the first nucleus and the O_1Z_1 axis. Then angles Θ_2 and Φ determine the orientation of the axial-symmetry axis of the second nucleus in the laboratory coordinate system O_2. Θ_2 is the angle between the axial-symmetry axis of the second nucleus and O_2Z_2 axis, and Φ is the angle between plane $X_2O_2Z_2$ and the plane formed by the axial-symmetry axis of the second nucleus and the O_2Z_2 axis. The angles Θ_2 and Φ are the Euler angles specifying the orientation of the coordinate system at rotation [42].

We consider the step proton density distributions in both nuclei as

$$\rho_i(\mathbf{r}) = \rho_{i0}\theta(R_i(\vartheta_i') - r), \tag{3}$$

where $\theta(x)$ is the step function and

$$R_i(\vartheta_i') = R_{i0}\left[1 + \sum_{\ell\geqslant 2}\beta_{i\ell} Y_{\ell 0}(\vartheta_i')\right] \tag{4}$$

is the distance of the deformed nuclear surface from the origin in an intrinsic (body-fixed) coordinate system O_i' of the nucleus i. Here R_{i0} and $\beta_{\ell i}$ are the radius and the deformation parameters, respectively, and ϑ_i' is the corresponding angle in the intrinsic coordinate system. The axis Z_i' of the intrinsic coordinate system O_i' coincides with the axial-symmetry axis of the nucleus i.

The angles Θ_1, Θ_2, and Φ are the Euler angles, which determine the rotation transformations between the intrinsic O_1' and O_2' and the laboratory coordinate systems O_1 and O_2, respectively. The transformation of spherical harmonic functions $Y_{\ell m}(\vartheta,\varphi)$ at rotation is described by the Wigner D functions $D^{\ell}_{m_1 m_2}(\Phi_1,\Theta,\Phi_2)$ [42]. Thus the distances of the deformed surfaces of nuclei from the origin of the coordinate systems O_1 and O_2 are

$$R_1(\vartheta_1,\varphi_1,\Theta_1) = R_{10}\left[1 + \sum_{\ell\geqslant 2}\beta_{1\ell}\sum_{m=-\ell}^{\ell} Y_{\ell m}(\vartheta_1',\varphi_1') D^{\ell}_{m0}(0,\Theta_1,0)\right], \tag{5}$$

$$R_2(\vartheta_2,\varphi_2,\Theta_2,\Phi) = R_{20}\left[1 + \sum_{\ell\geqslant 2}\beta_{2\ell}\sum_{m=-\ell}^{\ell} Y_{\ell m}(\vartheta_2',\varphi_2') D^{\ell}_{m0}(\Phi,\Theta_2,0)\right], \tag{6}$$

where ϑ_i' and φ_i' are the angles in the intrinsic coordinate system O_i', while ϑ_i and φ_i are the angles in the laboratory coordinate system O_i.

Substituting Eqs. (2)–(6) into Eq. (1), we can evaluate the integrals in Eq. (1). However, we can get a very cumbersome expression for the Coulomb energy of two nuclei if we take into account many terms in Eq. (2). Therefore, for the sake of simplicity, we should use reasonable approximations, which should not have much of an effect on the accuracy. Note that the values of the ground state quadrupole deformation parameter β_{i2} in stable nuclei are much larger than the ones for high-multipolarity cases $\beta_{i\ell}|_{\ell\geqslant 3}$ as a rule [44–47]. As a result, the values of the deformation parameters satisfy the condition $\beta_{i2}^2 \approx \beta_{i\ell}|_{\ell\geqslant 3}$. Therefore, we take into account the linear and quadratic terms of the quadrupole deformation parameters β_{i2} and the linear terms of the high-multipolarity deformation parameters $\beta_{i\ell}|_{\ell\geqslant 3}$. Using this approach, we obtain an expression for the Coulomb interaction of two axially

symmetric, arbitrarily oriented nuclei in the form

$$V_C(R, \Theta_1, \Theta_2, \Phi) = \frac{Z_1 Z_2 e^2}{R}\Bigg\{1 + \sum_{\ell \geqslant 2}[f_{1\ell}(R, \Theta_1, R_{10})\beta_{1\ell} + f_{1\ell}(R, \Theta_2, R_{20})\beta_{2\ell}] + f_2(R, \Theta_1, R_{10})\beta_{12}^2 + f_2(R, \Theta_2, R_{20})\beta_{22}^2 + f_3(R, \Theta_1, \Theta_2, R_{10}, R_{20})\beta_{12}\beta_{22} + f_4(R, \Theta_1, \Theta_2, \Phi, R_{10}, R_{20})\beta_{12}\beta_{22}\Bigg\}, \quad (7)$$

where Z_1 and Z_2 are the number of protons in corresponding nuclei, and

$$f_{1\ell}(R, \Theta_i, R_{i0}) = \frac{3R_{i0}^{\ell}}{(2\ell+1)R^{\ell}} Y_{\ell 0}(\Theta_i), \quad (8)$$

$$f_2(R, \Theta_i, R_{i0}) = \frac{6\sqrt{5}R_{i0}^2}{35\sqrt{\pi}R^2} Y_{20}(\Theta_i) + \frac{3R_{i0}^4}{7\sqrt{\pi}R^4} Y_{40}(\Theta_i), \quad (9)$$

$$f_3(R, \Theta_1, \Theta_2, R_{10}, R_{20}) = \frac{R_{10}^2 R_{20}^2}{R^4}\Bigg[-\frac{3}{20\pi} + \frac{3}{10\sqrt{5\pi}}(Y_{20}(\Theta_1) + Y_{20}(\Theta_2)) + \frac{51}{25}Y_{20}(\Theta_1)Y_{20}(\Theta_2)\Bigg] = \frac{27R_{10}^2R_{20}^2}{80\pi R^4}[17\cos^2(\Theta_1)\cos^2(\Theta_2) - 5\cos^2(\Theta_1) - 5\cos^2(\Theta_2) + 1], \quad (10)$$

$$f_4(R, \Theta_1, \Theta_2, \Phi, R_{10}, R_{20}) = \frac{R_{10}^2 R_{20}^2}{R^4}\Bigg\{\cos^2(\Phi)\Bigg[\frac{3}{10\pi} - \frac{3}{5\sqrt{5\pi}}(Y_{20}(\Theta_1) + Y_{20}(\Theta_2)) + \frac{6}{25}Y_{20}(\Theta_1)Y_{20}(\Theta_2)\Bigg] - \frac{27}{20\pi}\cos(\Phi)\sin(2\Theta_1)\sin(2\Theta_2)\Bigg\} = \frac{27R_{10}^2R_{20}^2}{40\pi R^4}[\cos^2(\Phi)\sin^2(\Theta_1)\sin^2(\Theta_2) - 2\cos(\Phi)\sin(2\Theta_1)\sin(2\Theta_2)]. \quad (11)$$

Here and below we take into account the volume correction that appeared in the second order on the quadrupole deformation parameter.

We see in Eqs. (7)–(11) that the Coulomb interaction of two deformed, axially symmetric nuclei depends on the orientation angles Θ_1, Θ_2, and Φ and consists of terms proportional to $\beta_{1\ell}$, β_{12}^2, $\beta_{2\ell}$, β_{22}^2, and $\beta_{12}\beta_{22}$. The next-order correction terms to Eq. (7) are negligible, because they are proportional to $\chi\beta_{i2}^3$ or $\chi\beta_{i2}^2\beta_{j2}|_{i\neq j}$, where $\chi \ll 1$ at $R > R_{10} + R_{20}$.

It is easy to see from Eq. (11) that if Θ_1 or Θ_2 equals 0 or π, then $f_4(R, \Theta_1, \Theta_2, \Phi, R_{10}, R_{20}) = 0$ for any Φ. This property shows that if the axial-symmetry axis of one nucleus coincides with the line connecting the mass centers of the nuclei (tip orientation of one nucleus and arbitrary orientation of another nucleus), then the rotation of another nucleus on any angle Φ does not affect either the mutual orientation or the Coulomb interaction energy of the nuclei.

The expression for the Coulomb interaction of two deformed axially symmetric nuclei depending on Θ_1, Θ_2, β_{12}, β_{12}^2, β_{22}, and β_{22}^2 has been discussed in Ref. [2]. However, Eqs. (7)–(11) contain more terms than are taken into account in Ref. [2]. The terms containing Φ have been ignored in all previously considered expressions for the Coulomb interaction of two deformed nuclei. The influence of angle Φ on the Coulomb interaction of deformed nuclei has been briefly discussed only in the framework of numerical calculations. The terms proportional to $\beta_{12}\beta_{22}$ have been taken into account in numerical calculations [30]. The functions f_i are proportional to the product of the integral of the radial form factor and the series of spherical harmonic functions in Ref. [30]. The dependence of total (Coulomb+nuclear parts) nucleus-nucleus potential on angle Φ has been numerically discussed for a few systems of deformed nuclei in Refs. [28,31].

The expression for the Coulomb interaction between spherical and deformed axially symmetric nuclei taking into account all linear and second-order terms on β_2, β_4, and β_6 multipole surface deformations is obtained in Ref. [5] see Eq. (B1) in this reference]. If we substitute $\beta_{12} = 0$ (or $\beta_{22} = 0$) in Eqs. (7)–(11) and leave only linear terms of $\beta_{i\ell>2} = 0$ in Eq. (B1) of Ref. [5], we can see that our expression and the expression from Ref. [5] are identical. This means that functions $f_{1\ell}(R, \Theta_i, R_{i0})$ and $f_2(R, \Theta_i, R_{i0})$ [see Eqs. (8) and (9)] coincide with the corresponding terms in Ref. [5].

III. THE NUCLEAR INTERACTION OF TWO AXIALLY SYMMETRIC NUCLEI

The expression for the nuclear part of the potential between spherical nuclei has been obtained in the semimicroscopic approach in Ref. [26]. The interaction energy of two nuclei equals the difference of the binding energies of the nucleus-nucleus system at finite and infinite distances between nuclei in this approach. The binding energy of the nuclear system is determined as a sum of kinetic and potential energies of nucleons. The kinetic energy is evaluated in the Thomas-Fermi approximation extended to the second-order gradient contributions. The potential energy is determined by the Skyrme energy-density functional for the SkM* parameter set. The kinetic and potential energies depend on the proton and neutron densities of both nuclei. The nucleon density distributions are obtained in the Hartree-Fock-BCS calculations for the Skyrme force parametrization SkM*. The distribution of nucleon densities in both nuclei are frozen during evaluation of the potential at different distances. The values of 7140 semimicroscopic frozen-density potentials between the set of

spherical nuclei from ^{16}O to ^{212}Po around touching points have been found numerically. The expression for the nuclear part of the potential is obtained by fitting the values of 7140 semimicroscopic potentials. The heights and radii of empirical fusion barriers are well described by this potential for various pairs of interacting nuclei [26,36,37].

We point out here that the approximation of the frozen distribution of nucleon densities is often used to evaluate the interaction between nuclei [24,30,48]. Thus the nucleus-nucleus potential used in the optical model can be written in the form [48]

$$U_{\rm opt}(R) = V_{00} + \sum_{jj'} V_{0j} \left[\frac{1}{E - H + i\varepsilon} \right]_{jj'} V_{j'0},$$

where V_{00} is the folding (or entrance-channel) nucleus-nucleus potential evaluated by using the effective nucleon-nucleon interaction and the ground-state nucleon densities, while the second term is the polarization potential, $\varepsilon \to +0$. The summation in the polarization term is over all possible combinations of excited states of both nuclei. The entrance-channel and polarization potentials are correspondingly the basic and correction contributions into the nucleus-nucleus potential.

We evaluate here and in Refs. [26,27] the entrance-channel potentials, which can be used in various optical model calculations as well as in other scattering problems, when contribution of the polarization potential is negligible. The frozen-density approximations may be applied to the evaluation of the potential around the touching point at such collision energies, when a time of density relaxation is larger than a time of barrier passing [27,49].

The nuclear part of the interaction potential between spherical nuclei is presented in Ref. [26] as the product of the mean reciprocal surface curvatures C_{12} of corresponding nuclei at the closest points and the function depending on the distance between mass centers. The distances between mass centers of nuclei R and between surfaces of nuclei at the closest point d are directly linked to each other. Therefore the shape of the potential obtained in Ref. [26] is similar to the proximity-type potential [38], and we can apply the proximity theorem to this potential.

According to the proximity theorem [38], the nuclear part of the interaction potential between deformed nuclei depends on both the smallest distance between nuclear surfaces $d(R, \Theta_1, \Theta_2, \Phi, R_{10}, R_{20}, \beta_1, \beta_2)$ and the mean reciprocal surface curvatures of the corresponding nuclei at the closest points. Therefore we approximate the nuclear part of the potential between deformed nuclei as

$$V_{\rm n}(R, \Theta_1, \Theta_2, \Phi) \approx \frac{C_{10} + C_{20}}{C_{\rm def}} V_{\rm n}^0(d^0(R_{\rm sph}, R_{10}, R_{20})), \tag{12}$$

where

$$C_{\rm def} = [(C_1^{\parallel} + C_2^{\parallel})(C_1^{\perp} + C_2^{\perp})]^{1/2} \tag{13}$$

is the generalized reciprocal curvature, and

$$d^0(R_{\rm sph}, R_{10}, R_{20}) = d(R, \Theta_1, \Theta_2, \Phi, R_{10}, R_{20}, \beta_1, \beta_2). \tag{14}$$

Here $V_{\rm n}^0(d^0(R_{\rm sph}, R_{10}, R_{20}))$ is the nuclear part of the interaction potential between spherical nuclei with radii R_{10} and R_{20} [26], $d^0(R_{\rm sph}, R_{10}, R_{20}) = R_{\rm sph} - R_{10} - R_{20}$ is the smallest distance between the surfaces of two spherical nuclei at distance $R_{\rm sph}$ between their mass centers, $C_{i0} = 1/R_{i0}$ is the curvature of the spherical surface of nucleus i, and $C_i^{\parallel}$ and $C_i^{\perp}$ are the main curvatures of the deformed surface of nucleus i at the point closest to the surface of another nucleus. Expressions for $V_{\rm n}^0(d^0(R_{\rm sph}, R_{10}, R_{20}))$ and $R_{1(2)0}$ are given in Ref. [26], and Eq. (13) for $C_{\rm def}$ is picked up from Ref. [50].

Ratio $(C_{10} + C_{20})/C_{\rm def}$ in Eq. (12) determines the dependence of the nucleus-nucleus potential strength on the deformations of surfaces at the closest point. For spherical nuclei, we have $C_i^{\parallel} = C_i^{\perp} = C_{i0}$ and $(C_{10} + C_{20})/C_{\rm def} = 1$.

The coordinates of the closest points of the surfaces, the curvatures of the nuclear surfaces at the closest points, and the distance between the closest points are found numerically for evaluation of the potential $V_{\rm n}(R, \Theta_1, \Theta_2, \Phi)$. At $R \geqslant R_{12}^0$, we determine exactly the closest distance between the surfaces of colliding nuclei $d(R, \Theta_1, \Theta_2, \Phi, R_{10}, R_{20}, \beta_1, \beta_2)$ and coordinates of the closest points $\theta'_{1,2}$ in the intrinsic coordinate systems, where

$$R_{12}^0 = R_{10} \left[1 + \sum_{\ell \geqslant 2} \beta_{1\ell} Y_{\ell 0}(\vartheta'_1) \right] \Bigg|_{\vartheta'_1 = 0} + R_{20} \left[1 + \sum_{\ell \geqslant 2} \beta_{2\ell} Y_{\ell 0}(\vartheta'_2) \right] \Bigg|_{\vartheta'_2 = \pi}.$$

At $R < R_{12}^0$, the nuclear surfaces can intersect. The numerical evaluation of the intersect distance is not straightforward. Therefore, for the sake of simplicity of the code, we approximate

$$d(R, \Theta_1, \Theta_2, \Phi, R_{10}, R_{20}, \beta_1, \beta_2) \approx \left(R - R_{12}^0\right) + d(R_{12}^0, \Theta_1, \Theta_2, \Phi, R_{10}, R_{20}, \beta_1, \beta_2)$$

at $R < R_{12}^0$, where $d(R_{12}^0, \Theta_1, \Theta_2, \Phi, R_{10}, R_{20}, \beta_1, \beta_2)$ is the distance between surfaces at distance $R = R_{12}^0$ for the same mutual orientation of the interacting nuclei.

The surface curvatures $C_i^{\parallel(\perp)}$ depend on the corresponding orientation angle(s) and deformation parameters. For the numerical evaluation of the surface curvatures in both nuclei with quadrupole and hexadecapole deformations, it is helpful

to use the expressions

$$C_1^{\parallel} = \kappa_1 + \kappa_1', \tag{15}$$

$$C_1^{\perp} = \kappa_1 - \kappa_1', \tag{16}$$

$$C_2^{\parallel} = \kappa_2 + \kappa_2' \cos(2\Phi), \tag{17}$$

$$C_2^{\perp} = \kappa_2 - \kappa_2' \cos(2\Phi), \tag{18}$$

$$\kappa_i(R_{i0}, \beta_{i\ell}, \vartheta') \approx C_{i0}\Bigg[1 + \sum_{\ell \geqslant 2} \frac{\ell(\ell+1)-2}{2} \beta_{i\ell} Y_{\ell 0}(\vartheta') - 5\beta_{i2}^2 (Y_{20}(\vartheta'))^2 + \frac{\beta_{i2}^2}{4\pi}\Bigg], \tag{19}$$

$$\kappa_i'(R_{i0}, \beta_{i\ell}, \vartheta') \approx -C_{i0}\frac{3}{8\pi}\sin^2(\vartheta')\big[2\sqrt{5\pi}\beta_{20} + 5\beta_{20}^2 - 30\cos^2(\vartheta')\beta_{20}^2 + 15\sqrt{\pi}\beta_{40}(7\cos^2(\vartheta') - 1)\big]. \tag{20}$$

Here ϑ' is the angle in the intrinsic coordinate system specifying the point on the nuclear surface, which is the closest to another nucleus. We use in Eqs. (17) and (18) the Euler theorem for the transformation of curvature at surface rotation [51]. The last term in brackets in Eq. (19) is induced by the volume conservation condition. Note that contributions with $\beta_{i\ell}|_{\ell>2}$ are absent in Eq. (20) because of the approximation $\beta_{i2}^2 \approx \beta_{i\ell}|_{\ell\geqslant 3}$, see Sec. II.

IV. THE INTERACTION OF AXIALLY SYMMETRIC NUCLEI AT VARIOUS RELATIVE ORIENTATIONS

The nucleus-nucleus interaction potential for zero value of orbital momentum is given as

$$V(R, \Theta_1, \Theta_2, \Phi) = V_{\mathrm{C}}(R, \Theta_1, \Theta_2, \Phi) + V_{\mathrm{n}}(R, \Theta_1, \Theta_2, \Phi). \tag{21}$$

Using Eqs. (7)–(21), we obtain the interaction potential between two arbitrarily oriented axially symmetric nuclei.

A. The accuracy of the potential evaluation

We limited our evaluation of the Coulomb interaction by the second-order terms on the quadrupole deformation and used an approximate method for calculation of the nuclear part of the potential. Therefore we should check the accuracy of our approximations.

The calculations of the potential between spherical and deformed nuclei in Ref. [27] are done using the numerical semimicroscopic approach. The proton and neutron densities in both nuclei are found in the framework of the Hartree-Fock-BCS model with SkM* set of Skyrme force parameters. The density evaluation is done with the condition that the calculated value of the nuclear electric quadrupole moment coincides with the experimental one [52] and that the ratio of the mass and electrical quadrupole moments of the nucleus is proportional to the ratio of the nucleons and protons in this nucleus. The nuclear part of the potential is evaluated using

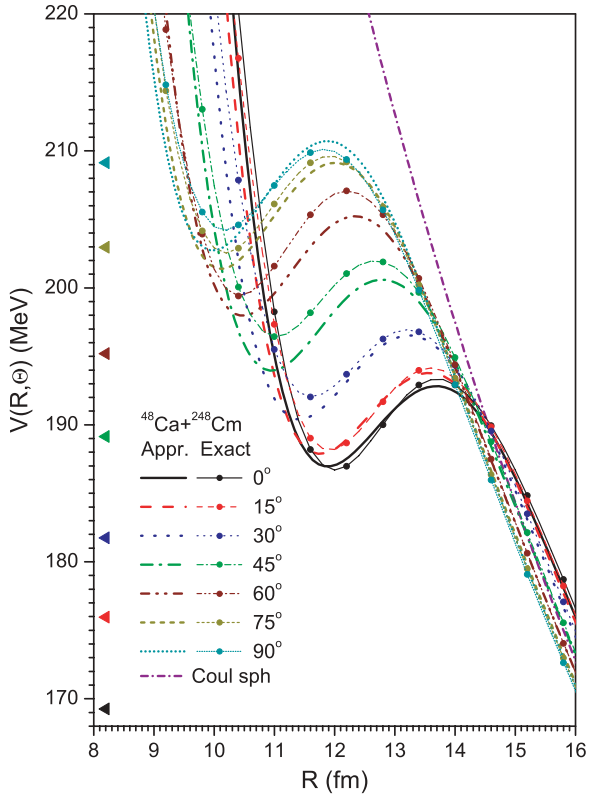

FIG. 2. (Color online) Entrance-channel interaction potentials for system ^{48}Ca+^{248}Cm evaluated with the SkM* Skyrme force. The potentials are evaluated for different angular orientations of the heavy deformed nuclei (Θ_2). The lines without dots are obtained using Eqs. (7)–(21). The lines with dots correspond to exact numerical calculations from Ref. [27]. For reference, the Coulomb potential is presented, too. The ground-state Q value is indicated by the lowest triangle at the left vertical axis. The other six triangles mark, respectively, the thresholds for the emission of 1, 2, 3, 4, 5, and 6 neutrons. The ground-state Q value and the thresholds for the neutron emission are evaluated by using the atomic masses from Ref. [53].

the extended Thomas-Fermi approximations and the Skyrme energy-density functional. The Coulomb interaction of two nuclei is evaluated numerically taking into account the direct and exchange contributions and using the Hartree-Fock-BCS proton densities in both nuclei. The nucleus-nucleus entrance-channel potential is evaluated using frozen nucleon densities in both nuclei.

We compare in Fig. 2 the entrance-channel nucleus-nucleus potentials for the system ^{48}Ca+^{248}Cm evaluated in the framework of exact numerical and approximate [using Eqs. (7)–(21)] semimicroscopic methods at various distances R and orientation angles Θ. The values of the quadrupole moment of curium and the set of Skyrme force parameters are the same in the both calculations. We especially give attention to the distances around the touching and barrier points, which are very important to the capture process and SHE production [27]. The potentials quickly converge to the Coulomb interaction of two point nuclei at larger distances, because the nuclear interaction is exponentially attenuated at large distances and the correction terms of the Coulomb

interaction induced by deformation of ^{248}Cm are reduced according to the law $(R_{^{248}\mathrm{Cm}}/R)^2$ [see Eqs. (8) and (9)], where $R_{^{248}\mathrm{Cm}}$ is the radius of ^{248}Cm in the case of a spherical shape.

We see in Fig. 2 that the values of barriers evaluated in both models agree very well for various orientations of deformed nucleus. The largest difference between the barrier values obtained in these approaches is less than 2 MeV at $\Theta_2 \approx 45^\circ$–$60^\circ$. This difference is close to 1% of the barrier height. In comparison to this, the differences between barrier values estimated in various approaches [26,38,54–57] for spherical colliding systems leading to heavy and superheavy nuclei are close to 10 MeV or 5% of the barrier height [27,37,49]. The agreement between values of potentials around the barriers in Fig. 2 is much better for smaller $\Theta_2 \leqslant 30^\circ$ and larger $\Theta_2 \geqslant 75^\circ$ angles.

The strong repulsion appears in potentials at very small distances between nuclei in Fig. 2. This repulsion is induced by the appreciable overlapping of nucleon densities belonging to colliding nuclei. The exact and approximate potentials for various orientations are very close to each other at very small distances too.

As a result, the accuracy of the entrance-channel potential at various orientations evaluated using the approximate expression is high. Therefore we can apply our method for the calculation of the interaction energy between various deformed, arbitrarily oriented nuclei.

B. Comparative study of potentials for prolate-prolate, prolate-oblate, and oblate-oblate systems

The depth and width of capture well (pocket) and barrier height play crucial roles in the compound-nucleus formation in fusion reactions [27]. Therefore it is necessary to study the deformation dependence of the entrance-channel nucleus-nucleus potential around the touching point.

The influence of various deformations on the interaction potential is exemplified by detailed consideration of the system ^{86}Kr+^{86}Kr. The ground-state shape of ^{86}Kr is spherical [44,45,52]. However, we change the shape of interacting nuclei for the sake of obtaining the peculiarities of the potential induced by both the various orientations of incoming nuclei and the deformations of different types. The nucleus-nucleus potentials for the systems $^{86}\mathrm{Kr}(\beta_{12} = 0.25)+^{86}\mathrm{Kr}(\beta_{22} = 0.25)$ (prolate-prolate), $^{86}\mathrm{Kr}(\beta_{12} = 0.25)+^{86}\mathrm{Kr}(\beta_{22} = -0.25)$ (prolate-oblate), and $^{86}\mathrm{Kr}(\beta_{12} = -0.25)+^{86}\mathrm{Kr}(\beta_{22} = -0.25)$ (oblate-oblate) for various orientations are presented in Fig. 3.

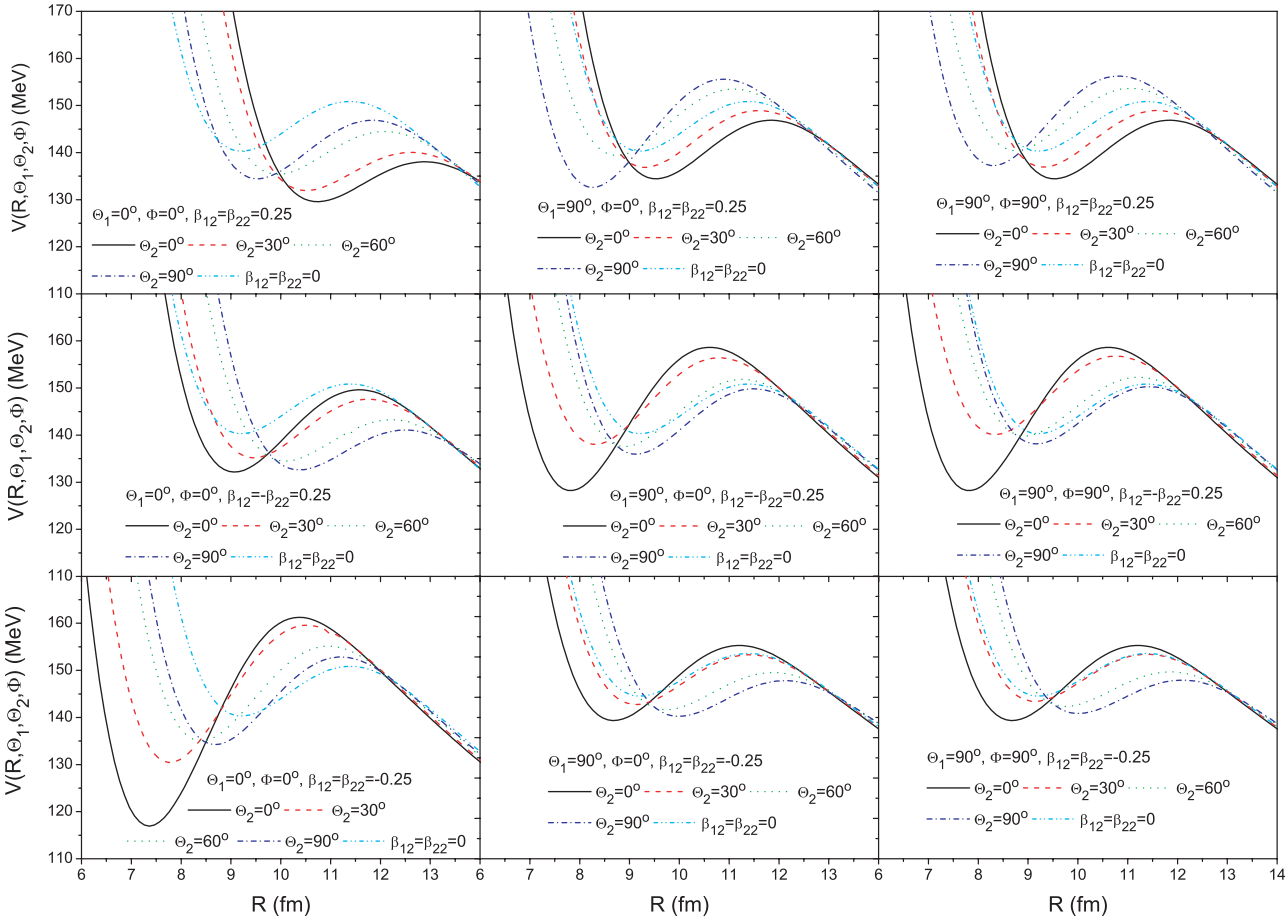

FIG. 3. (Color online) Nucleus-nucleus potentials for the systems $^{86}\mathrm{Kr}(\beta_{12} = 0.25)+^{86}\mathrm{Kr}(\beta_{22} = 0.25)$, $^{86}\mathrm{Kr}(\beta_{12} = 0.25)+^{86}\mathrm{Kr}(\beta_{22} = -0.25)$, and $^{86}\mathrm{Kr}(\beta_{12} = -0.25)+^{86}\mathrm{Kr}(\beta_{22} = -0.25)$ for various orientations. The potential between spherical nuclei for the system $^{86}\mathrm{Kr}(\beta_{12} = 0)+^{86}\mathrm{Kr}(\beta_{22} = 0)$ is also presented on each panel.

For reference, the potential between the spherical nuclei ^{86}Kr($\beta_{12} = 0$)+^{86}Kr($\beta_{22} = 0$) is also given in each panel of Fig. 3. The charges and numbers of nucleons in both nuclei are the same for any potential in Fig. 3, therefore the differences between potentials are only induced by both the deformation type and the mutual orientation of interacting nuclei.

The potentials for the prolate-prolate (oblate-oblate) system evaluated at $\Theta_1 = 0^\circ$ and $\Theta_2 = 90^\circ$ in the left panel, at $\Theta_1 = 90^\circ$, $\Theta_2 = 0^\circ$, and $\Phi = 0^\circ$ in the middle panel, and at $\Theta_1 = 90^\circ$, $\Theta_2 = 0^\circ$, and $\Phi = 90^\circ$ in the right panel are the same due to symmetry of the interacting system.

Comparing the potentials in Fig. 3, the following features are observed:

(i) Shape of the capture well and barrier height strongly depend on both the mutual orientation of colliding nuclei and the type of deformation.

(ii) The lowest barrier height and the shallowest capture well take place for tip-tip ($\Theta_1 = \Theta_2 = 0^\circ$) orientation of the prolate-prolate system. This orientation of prolate nuclei corresponds to the most extended system around barrier.

(iii) The highest barrier height and the deepest capture well take place for tip-tip ($\Theta_1 = \Theta_2 = 0^\circ$) orientation of the oblate-oblate system. This orientation of oblate nuclei relates to the most compact system around barrier.

(iv) The barrier radius for tip-tip orientation of prolate-prolate system is the largest one, while the one for tip-tip orientation of oblate-oblate system is the smallest one.

(v) The difference between the lowest and highest barriers caused by mutual orientation of prolate nuclei is larger then the one induced by mutual orientation of oblate nuclei. In contrast to this, the difference between the lowest and highest positions of the bottom of capture wells caused by mutual orientation of oblate nuclei is larger than the one induced by the mutual orientation of prolate nuclei. Therefore prolate deformation is more important for the barrier heights, while oblate deformation is more important for the properties of the capture well.

(vi) The compact nucleus-nucleus systems around the touching point have a deeper capture well, higher barrier, and larger curvature of the potential at the barrier, while the extended colliding systems have smaller values of the depth of the capture well, barrier height, and the curvature of the potential at the barrier.

(vii) The difference between side-side potentials ($\Theta_1 = \Theta_2 = 90^\circ$) evaluated at various values of Φ ($\Phi = 0^\circ$ and $\Phi = 90^\circ$) is negligible for the barrier and noticeable for capture well. This difference is especially important for the prolate-prolate colliding systems. The small dependence of the potential barrier on Φ is mainly induced by the variation of the Coulomb potential, which slightly varies with Φ.

(viii) The more compact system is more easily fusing, because

(a) the capture well is deeper, therefore more states of the two-nuclear system can be located around the collision energy and populated during capture and consequent processes leading to the compound-nucleus;

(b) the force driving the touching nuclei to compound-nucleus formation and connected with the gradient of the entrance-channel potential at distances between the barrier radius and the radius of the bottom of the capture well is larger; and

(c) the thickness of barrier is smaller, because the curvature of the potential at the barrier point is smaller. This particularity is especially important for subbarrier fusion reactions.

(ix) The more extended system is more easily separated into fragments, because the capture well is shallow and the driving force to compound-nucleus formation is relatively small. Taking into account that the barrier height is the lowest for the most extended shape, it is clear why fission fragments formed after neck rupture are well-prolate.

(x) The orientations leading to the easiest heavy-ion fusions at high energies are $\Theta_1 = \Theta_2 = 90^\circ$ and $\Phi = 0^\circ$ for the prolate-prolate system; $\Theta_1 = 90^\circ$, $\Theta_2 = 0^\circ$, and any values of Φ for the prolate-oblate system; and $\Theta_1 = \Theta_2 = 0^\circ$ and any values of Φ for the oblate-oblate system.

The barrier heights and radii are related to the balance between repulsive Coulomb potential and attractive nuclear interactions between nuclei. The nuclear interaction is very short-ranged and noticeable only at small distances between surfaces of two nuclei. The Coulomb force is long-ranged and weakly depends on distance between surfaces of two nuclei. Therefore the barrier height for deformed nuclei strongly depends on orientation of incoming nuclei. The nuclear part of interaction for extended nucleus-nucleus system is noticeable at relatively large distances between mass centers of colliding nuclei R. The Coulomb interaction $\approx Z_1 Z_2 e^2/R$ reduces with growing R. As a result, the barrier height is smaller for extended shapes of nucleus-nucleus system. The opposite case is the compact shape of the nucleus-nucleus system. The compact nucleus-nucleus shape is related to the smallest barrier radius and the highest barrier value.

The difference between the lowest and highest barriers induced by mutual orientation of deformed nuclei rises with deformation values.

The depth of the capture well is strongly related to the strength of the nuclear force between colliding nuclei. If the domain related to the range of strong nuclear interaction of nuclei rises, then the strength of nuclear interaction increases too. The dependence of the nuclear interaction on the magnitude of the nuclear interaction domain is described by the ratio of surface curvatures $(C_{10} + C_{20})/C_{\rm def}$ in Eq. (12). The smaller value of the surface curvature corresponds to a larger area of the strong interaction. The values of the nuclear interaction between heavy ions at the same distances between the closest points are inversely related to the generalized curvature $C_{\rm def}$. The largest domain of nuclear force between prolate nuclei is related to the side-side orientation, where the surface curvatures in the closest points are the smallest [see Eqs. (15)–(20)], while the smallest one is linked with the

tip-tip orientation, where the surface curvatures in the closest points are the largest. Because of this, the capture well for the side-side orientation of incoming prolate nuclei is deeper than the one for the tip-tip orientation of these nuclei.

The ground-state Q value of the compound-nucleus ^{172}Hf formed in the fusion ^{86}Kr+^{86}Kr is 110.13 MeV. Here we use the experimental binding energies of nuclei [53] for evaluating the reaction Q value. Both the barrier heights and the bottoms of the capture wells presented in Fig. 3 are well above the ground-state energy of the compound nucleus. The final value of the collective coordinate R can be defined as the distance $R_f = \frac{3}{4}R^0_{\rm CN} \approx 5$ fm between the mass centers of the left and right hemispheres of the compound nucleus, where $R^0_{\rm CN} = r_0 A^{1/3}$ is the radius of the spherical compound nucleus with A nucleons. Therefore the adiabatic fusion potential smoothly connecting the entrance-channel potential at distances close to the touching distance with the ground-state reaction Q value at R_f exhibits a large gradient driving the system into the compound-nucleus shape for any orientation as well any deformation type of the incoming nuclei. Consequently, the compound nucleus should be formed in the fusion ^{86}Kr+^{86}Kr after barrier passing.

C. Potentials for systems leading to SHE

1. *Potentials for very asymmetric systems leading to SHE*

The values of the SHE production cross section are very small [7–11,13–20]. Therefore the nuclei participating in fusion reactions leading to the SHE and the collision energies are very carefully selected [7]. The collision energies used in the reaction leading to SHE should be above or slightly below the fusion barrier heights for obtaining the high values of the capture cross section, because the probability of barrier transmission is strongly reduced at subbarrier collision energies. On the other hand, the excitation energies of the compound-nucleus formed in the reaction should be as small as possible because of the competition between fission and neutron emission [58]. A large number of neutrons emitted from the compound nucleus reduces the SHE formation cross section. The excitation energy of the compound nucleus equals the difference between the collision energy and the ground-state reaction Q value. Thus ratios between the collision energy, the fusion barrier values, the ground-state reaction Q value, the fission barrier value of the compound nucleus, and the thresholds for neutron emission are especially important for the SHE formation in nucleus-nucleus collisions. Below we discuss specific properties of the reactions used in various experiments with ^{19}F, ^{22}Ne, and ^{26}Mg projectiles on heavy targets.

The reaction ^{19}F+^{248}Cm $\rightarrow$ ^{262}Db+5n is often studied experimentally [14]. Both nuclei participating in this reaction are prolate [44,45,52]. The values of the ground-state quadrupole β_2 and hexadecapole β_4 deformation parameters for these nuclei are given in Table I.

The values of deformation parameters obtained in various models and extracted from experimental data for the same nuclei are well scattered as a rule (see Table I). Therefore if the experimental value of the quadrupole deformation parameter is unknown for heavy nuclei ($A > 40$), then we evaluate the nucleus-nucleus potential at $\beta_2^\circ = (\beta_2^{\rm mm} + \beta_2^{\rm mic})/2$. Here $\beta_\ell^{\rm mm}$ and $\beta_\ell^{\rm mic}$ are, respectively, the values of deformation parameters obtained in the framework of the macro-microscopic model (the finite-range droplet model with the Strutinsky shell corrections) [44] and the Hartree-Fock-BCS theory with the Skyrme force parameter set MSk7 [45].

The reduced probabilities $B(E2)$ are basic experimental quantities that do not depend on the nuclear models. The experimental value of the quadrupole deformation $\beta_2^{\rm exp}$ presented in Table I is obtained by using the formula [52]

$$\beta_2^{\rm exp} = \frac{4\pi}{3ZR_p^2}[B(E2)/e]^{1/2}, \tag{22}$$

where $R_p = 1.2A^{1/3}$ fm is the proton radius.

To calculate the nucleus-nucleus potential, we take into account terms with β_2, β_2^2, and β_4 and define the proton radius parameter as $R_p^{\rm pot} = 1.24[1+1.646/A-0.191(A-2Z)/A]A^{1/3}$ [26]. Therefore we should use the same approximation and radius value to evaluate the ratio between the reduced probability $B(E2)$ and the parameter of the quadrupole deformation. As a result, the value of the quadrupole deformation β_2° in our approximation should be evaluated from the equation

$$\beta_2^\circ + \frac{2\sqrt{5}}{7\sqrt{\pi}}(\beta_2^\circ)^2 = \frac{4\pi}{3Z\left(R_p^{\rm pot}\right)^2}[B(E2)/e]^{1/2}. \tag{23}$$

Comparing Eqs. (22) and (23), we find that

$$\beta_2^\circ + \frac{2\sqrt{5}}{7\sqrt{\pi}}(\beta_2^\circ)^2 = \frac{R_p^2}{\left(R_p^{\rm pot}\right)^2}\beta_2^{\rm exp}. \tag{24}$$

This equation clearly shows the origin of the different values extracted from experimental data for $B(E2)$ given in the sixth and the seventh columns in Table I.

The experimental values of the hexadecapole deformation parameter are unknown, thus we use $\beta_4^\circ = (\beta_4^{\rm mm} + \beta_4^{\rm mic})/2$ for medium and heavy nuclei ($A \gtrsim 40$) at calculations of the interaction potentials. Various theoretical models [44–47] predict appreciably different values of deformation parameters for light nuclei. Therefore we put $\beta_4^\circ = 0$ for light nuclei ($A \lesssim 40$). The experimental value of the quadrupole deformation parameter for ^{19}F is unknown; therefore we use the value of this parameter from the Hartree-Fock-BCS theory [45]. We consider that the Hartree-Fock-BCS model is a more realistic approach to light nuclei than the macro-microscopic model.

The potentials for the system ^{19}F+^{248}Cm leading to Db for various orientations are presented in Fig. 4. The collision energy in the middle of the target used in the experiment for the synthesis of Db is $E_{\rm c.m.} \approx 99$ MeV [14]. We see that the experimental collision energy is smaller than the barrier for the side-side orientation of colliding nuclei (see the middle and right upper panels in Fig. 4) and very close to the barrier for the tip-side orientation (see the left upper panel in Fig. 4). The barrier for the tip-tip orientation of fusing nuclei is located approximately 9 MeV below the experimental collision energy.

TABLE I. Ground-state quadrupole β_2 and hexadecapole β_4 deformation parameters of nuclei. Here β_2° and β_4° are the values of deformation parameters used in the evaluation of the nucleus-nucleus potential; $\beta_{\ell=2,4}^{\rm mm}$ and $\beta_{\ell=2,4}^{\rm mic}$ are, respectively, the values of deformation parameters obtained in the frameworks of the macro-microscopic model [44] and the Hartree-Fock-BCS model [45]; $\beta_2^{\rm exp}$ is the experimental value of the quadrupole deformation extracted in linear approximation of the deformation parameter from the compilation [52].

Nucleus	$\beta_2^{\rm mm}$	$\beta_4^{\rm mm}$	$\beta_2^{\rm mic}$	$\beta_4^{\rm mic}$	$\beta_2^{\rm exp}$	β_2°	β_4°
^{19}F	0.275	0.307	0.23	0.00	–	0.23	0.00
^{22}Ne	0.326	0.225	0.40	−0.04	0.562	0.410	0.00
^{26}Mg	−0.310	0.186	−0.32	−0.05	0.482	0.363	0.00
^{64}Zn	0.219	−0.031	−0.18	−0.02	0.242	0.2053	−0.0255
^{70}Zn	0.045	0.001	0.00	0.00	0.228	0.2006	0.0005
^{232}Th	0.207	0.108	0.22	0.03	0.2608	0.2416	0.0690
^{238}U	0.215	0.093	0.24	0.02	0.2863	0.2637	0.0565
^{244}Pu	0.224	0.062	0.23	0.01	0.2931	0.2698	0.0360
^{241}Am	0.223	0.087	0.25	0.01	–	0.2365	0.0485
^{243}Am	0.224	0.071	0.24	0.01	–	0.232	0.0405
^{248}Cm	0.235	0.040	0.28	−0.02	0.2972	0.273	0.0100
^{249}Bk	0.235	0.040	0.28	−0.02	–	0.2575	0.0100
^{249}Cf	0.235	0.033	0.25	0.00	–	0.2425	0.0165
^{250}Cf	0.245	0.026	0.28	−0.02	0.299	0.2735	0.0030

The difference between the barriers of entrance-channel potentials for the same values of angles $\Theta_{1,2}$ and different values of angle Φ can be studied by comparing results in the middle and right panels of Fig. 4. We conclude that the influence of heavy nucleus rotation related to angle Φ is negligible for barrier heights and values of potentials at large distances between very asymmetric nuclear systems. The variation of angle Φ is weakly noticeable for the depth of the capture well. The capture well at $\Theta_1 = \Theta_2 = 90^\circ$ and $\Phi = 0^\circ$ is approximately 3 MeV deeper than the one at $\Theta_1 = \Theta_2 = 90^\circ$ and $\Phi = 90^\circ$.

A shallow capture well is observed at the tip orientation of ^{19}F, see the left panel in Fig. 4. The small radius of the tip (or large value of surface curvature) in well-deformed ^{19}F induces the reduction of the strong interaction domain, therefore the attraction force between colliding nuclei is reduced. The depth of the capture well at fixed value Θ_2 increases with Θ_1.

The capture wells of entrance-channel potential for the reaction ^{19}F+^{248}Cm at orientations $\Theta_1 = 90^\circ$ and $\Theta_2 = 60^\circ$–90° are the deepest and, therefore, the most important for the capture process. The capture well depth for incoming spherical nuclei is larger than the one for the tip-tip orientation but smaller than the one for the side-side orientation of deformed nuclei. Therefore the side-side orientation of deformed nuclei enhances the capture well depth and, as a result, the compound-nucleus formation.

We see in Figs. 3 and 4 that potentials at orientations $\Theta_1 = \Theta_2 = 0^\circ$ and $\Theta_1 = \Theta_2 = 90^\circ$ and $\Phi = 0^\circ$ contain the most essential information on the range of barrier heights and properties of capture wells, so we will discuss below the dependence of the potentials on angle Φ only in specific cases.

The entrance-channel nucleus-nucleus potentials for various orientations of colliding nuclei for reactions induced by ^{22}Ne beam on very heavy targets ^{232}Th, ^{238}U, ^{244}Pu, ^{241,243}Am, ^{248}Cm, ^{249}Bk, and ^{249,250}Cf are presented in Fig. 5. The entrance-channel potentials for reactions between ^{26}Mg projectile and the same set of very heavy targets at various orientations are given in Fig. 6. Note that reactions ^{22}Ne+^{232}Th [13], ^{22}Ne+^{238}U [15], ^{22}Ne+^{244}Pu [12,15], ^{22}Ne+^{241}Am [17], ^{22}Ne+^{248}Cm [11], ^{22}Ne+^{249}Bk [16], ^{26}Mg+^{238}U [15], ^{26}Mg+^{243}Am [19] and ^{26}Mg+^{248}Cm [18] have been successfully used in various laboratories for synthesis of SHE. The values of the surface deformation parameters of the nuclei in the evaluation of the potentials are presented in Table I.

Comparing results for the entrance-channel potentials at various orientations in Fig. 4–6 for very asymmetric systems, we can conclude that

(i) Deformation and orientation of nuclei change drastically the shape of the nucleus-nucleus potential. The barrier height, bottom of the capture well, capture well width, and gradient of the capture well driving the nucleus-nucleus system to the compound nucleus strongly depend on the orientation of the incoming deformed nuclei.

(ii) The tip-tip orientation of colliding nuclei is related to the lowest barrier value, shallowest capture well, and most elongated shape of nuclei around the barrier and capture well. In contrast to this, the side-side orientation of fusing nuclei is connected to the highest barrier value, deepest capture well, and most compact shape of nucleus-nucleus system.

(iii) Because of the various incoming orientations, the entrance-channel barrier heights are distributed over the wide range. The difference between the highest and lowest values of barrier height is close to 10–15 MeV. As a result, three to six neutrons can evaporate from compound nuclei at energies close to the barriers at various orientations of colliding nuclei. Therefore various

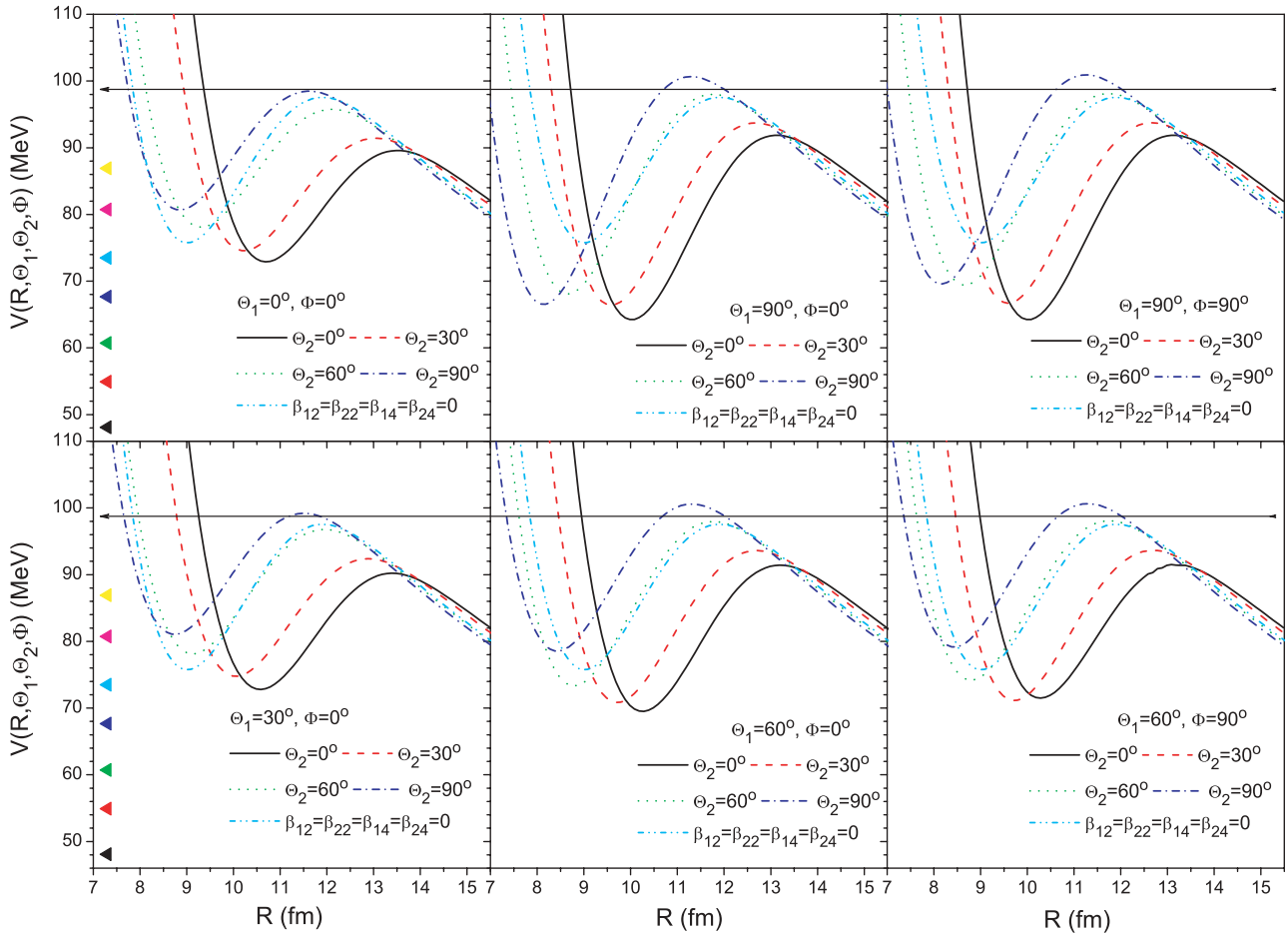

FIG. 4. (Color online) Nucleus-nucleus potentials for the system ^{19}F+^{248}Cm for various orientations. The potential between spherical nuclei for the system ^{19}F+^{248}Cm is also presented on each panel. The ground-state Q values are indicated by the lowest triangles at the left vertical axes. The other six triangles mark, respectively, the thresholds for the emission of 1, 2, 3, 4, 5, and 6 neutrons. The horizontal arrow indicates the collision energy used in the experiment.

neutron emission channels can be studied in reaction by choosing the collision energies.

(iv) Deformation and orientation of a light nucleus is less important to the barrier position than the ones of a heavy nucleus. In contrast to this, the deformation and orientation of a light nucleus are very significant to capture well properties. The position of the bottom of the capture well strongly depends on the orientation of the light nucleus.

(v) The side orientation of incoming nuclei is related to the highest values of barrier heights, five to six neutron emission channels, and the highest values of the gradient of capture well driving the nucleus-nucleus system to the compound nucleus. As a result, such nucleus-nucleus orientation easy leads to the highly excited compound nucleus, but the SHE formation cross section is reduced by strong competition between the neutron evaporation and the fission of the compound nucleus.

(vi) The tip orientation of a heavy nucleus in the entrance channel leads to the smallest values of barrier heights, three to four neutron emission channels, and the smallest values of the gradient of capture well driving the nucleus-nucleus system to the compound nucleus. Such nucleus-nucleus orientation leads to moderate competition between the evaporation of neutrons and the fission of the compound nucleus, but the probability of compound-nucleus formation is, probably, smaller than the one for the side-side orientations. Therefore searching for the collision energy leading to the best balance between the compound-nucleus formation and compound-nucleus survival is the most important task for the synthesis of SHE.

(vii) The isotopic dependence of the nucleus-nucleus entrance-channel potential induced by small variation of atomic mass is related to both the variation of radii and the changing of the values of surface deformation parameters. The isotopic variation of the deformation parameters is a leading factor in the properties of the entrance-channel potential, especially for the positions of both the barrier height and the bottom of the capture well.

(viii) The entrance-channel potentials between light well-deformed and heavy deformed nuclei show the deep capture well at orientations $\Theta_1 = 90^\circ$, $\Theta_2 = 60^\circ$–90°.

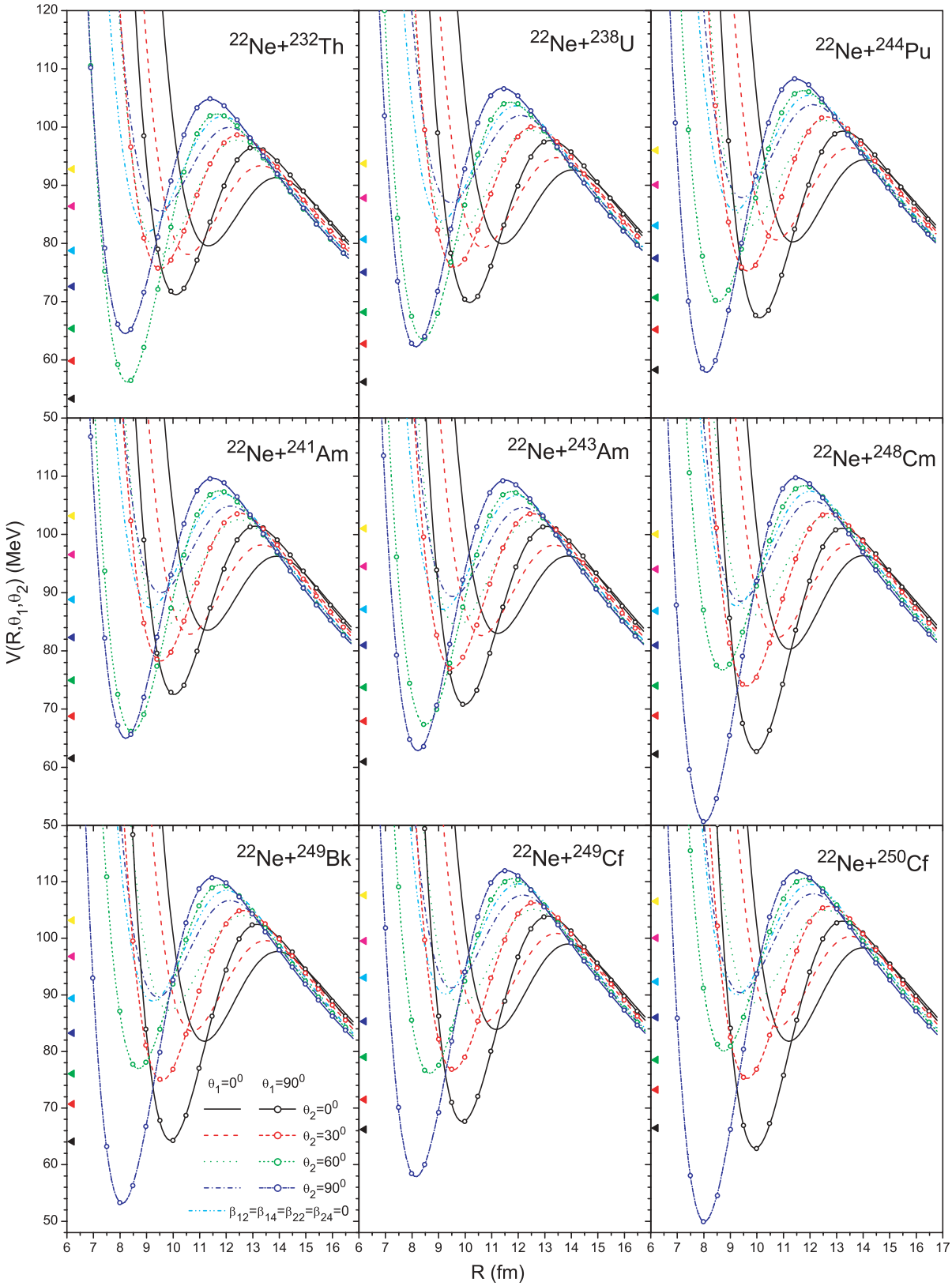

FIG. 5. (Color online) Nucleus-nucleus potentials for the systems ^{22}Ne+^{232}Th, ^{22}Ne+^{238}U, ^{22}Ne+^{244}Pu, ^{22}Ne+^{241,243}Am, ^{22}Ne+^{248}Cm, ^{22}Ne+^{249}Bk, and ^{22}Ne+^{249,250}Cf at various orientations of incoming nuclei. The potential between spherical nuclei ($\beta_{12} = \beta_{14} = \beta_{22} = \beta_{24} = 0$) for each system is also presented on each panel. The ground-state Q values are indicated by the lowest triangles at the left vertical axes. The other six triangles mark, respectively, the thresholds for the emission of 1, 2, 3, 4, 5, and 6 neutrons.

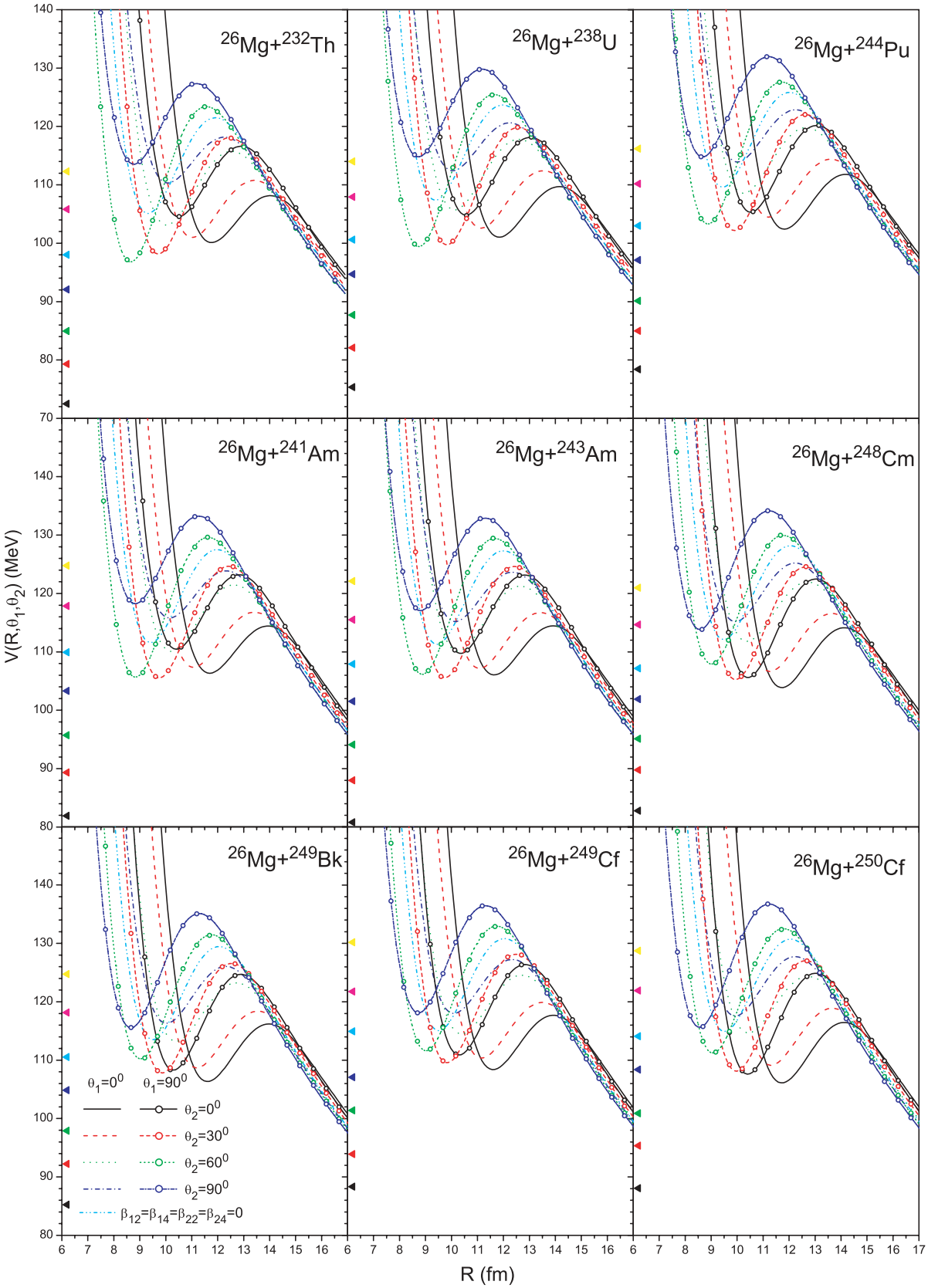

FIG. 6. (Color online) Nucleus-nucleus potentials for the systems ^{26}Mg+^{232}Th, ^{26}Mg+^{238}U, ^{26}Mg+^{244}Pu, ^{26}Mg+^{241,243}Am, ^{26}Mg+^{248}Cm, ^{26}Mg+^{249}Bk, and ^{26}Mg+^{249,250}Cf at various orientations of incoming nuclei. The potential between the spherical nuclei ($\beta_{12} = \beta_{14} = \beta_{22} = \beta_{24} = 0$) for each system is also presented on each panel. The notations are the same as in Fig. 5.

This particularity can be used for the synthesis of SHE, because the shape of the nuclear system at such orientations is the most compact.

2. Barrier heights for the side-tip and side-side orientations and SHE production

It has been established experimentally that there is fusion hindrance for the tip-tip orientation of weakly mass-asymmetric heavy colliding systems [59]. The fusion hindrance for the tip orientation for the strongly mass-asymmetric system ^{16}O+^{238}U is also observed in Ref. [60]. However, similar properties of complete fusion for the tip and side orientations have been found recently for reaction ^{16}O+^{238}U by another experimental group [61]. Moderate (∼80%) fusion hindrance for the tip-tip orientation has been observed very recently for reaction ^{30}Si+^{238}U $\rightarrow^{268-x}$ Sg + xn [62]. Therefore if strong fusion hindrance is absent in the collision of a very asymmetric system, then it is very promising to form SHE in such a system.

Thus SHE production and fusion-fission cross sections have been measured for the reaction ^{22}Ne+^{248}Cm in a wide range of collision energies [11]. The cross-section value for the reaction channel ^{22}Ne+^{248}Cm $\rightarrow^{266}$ Sg + 4n measured at the collision energy ∼106 MeV is larger than the one at ∼111 MeV. However, the highest value of the cross section for this reaction pair has been obtained for the channel ^{22}Ne+^{248}Cm → ^{265}Sg + 5n at an energy of ∼111 MeV. Therefore the SHE production cross sections for reaction ^{22}Ne+^{248}Cm are high enough at energies higher than the side-tip barrier, see Fig. 5. The highest values of the cross sections are related to the orientations forming the deepest capture well or to the energy interval corresponding to the barriers at orientations $\Theta_1 \sim 90^\circ$, $60^\circ \lesssim \Theta_2 \lesssim 90^\circ$. The SHE formation at energies between the side-tip and side-side entrance-channel barriers is very favorable. However, the SHE formation cross section decreases at very high collision energies due to the strengthening of the competition between fission and neutron emission. The SHE production cross section at energies in the interval between the tip-tip ($\Theta_1 = \Theta_2 = 0^\circ$) and side-tip barriers should be smaller because of the smaller capture pocket depth and, as a result, the increase in the fusion hindrance. The formation of SHE at energies below the tip-tip barrier is additionally suppressed by the small value of the barrier transmission.

The fission cross section of ^{270}Sg formed in the reaction ^{22}Ne+^{248}Cm goes down by 1500 times when the collision energy is reduced from 116.7 to 93.7 MeV [11]. The lower collision energy is just below the tip-tip barrier, while the higher collision energy exceeds the side-side barrier height. Taking into account the observed reduction of the fusion cross section, we conclude that orientations $\Theta_1 \sim 90^\circ$, $60^\circ \lesssim \Theta_2 \lesssim 90^\circ$ lead to the compound nucleus, while the compound-nucleus formation is suppressed at the tip-tip orientations.

Note that the reaction ^{19}F+^{248}Cm →Db has been successfully studied at energies between the side-tip and side-side barriers too, see Fig. 4. Moreover, reactions induced by the collision of ^{22}Ne+^{232}Th [13], ^{22}Ne+^{238}U [15], ^{22}Ne+^{244}Pu [12,15], ^{22}Ne+^{241}Am [17], ^{22}Ne+^{248}Cm [11], ^{22}Ne+^{249}Bk [16], ^{26}Mg+^{238}U [15], ^{26}Mg+^{243}Am [19], and ^{26}Mg+^{248}Cm [18] leading to SHE are also done at energies around the side-side barrier height, but higher than the side-tip barrier height. Therefore the available SHE formation data induce further study of SHE production in very asymmetric reactions at collision energy intervals between the side-tip and side-side barriers.

The SHE production in the reactions ^{22}Ne+^{249}Cf and ^{26}Mg+^{249}Cf leading, correspondingly, to $^{275}_{108}$Hs$_{163}$ and $^{275}_{110}$Da$_{165}$ compound nuclei at energies close to or below the side-side entrance-channel barrier can be very promising. The SHE formed in these reactions are more neutron-rich than those obtained in cold-fusion reactions [7]. The values of the fission barriers in isotopes Hs and Da have a maximum at neutron numbers of 161 and 163, respectively [63]. Both the spontaneous-fission and α-decay half-lives have local maximums for isotopes Hs and Da around a number of neutron $N = 162$ [64]. Therefore compound nuclei formed in these reactions are relatively stable. As a result, the experiments for SHE production in the reactions ^{22}Ne+^{249}Cf and ^{26}Mg+^{249}Cf at energies close to or below the side-side entrance-channel barrier are very desirable.

3. Potentials for the system leading to SHE with $Z = 120, 122$

Using the hot-fusion reaction ^{48}Ca + X, where X is a heavy transuranium element, SHE with $Z = 112$–118 have been synthesized in Dubna and Darmstadt laboratories [7,65]. However, reactions with the ^{48}Ca beam are limited by the availability of heavy transuranium elements. The heaviest element with 118 protons has been formed in the reaction ^{48}Ca+^{249}Cf [65]. Because more heavy targets are practically unavailable, it is necessary to search for other possibilities for synthesis of SHE with $Z > 118$. We show below that reactions ^{64,70}Zn+^{232}Th and ^{64,70}Zn+^{238}U are very promising for SHE production with 120 and 122 protons.

In Fig. 7, we present results for entrance-channel potentials for systems ^{64,70}Zn+^{232}Th and ^{64,70}Zn+^{238}U at various orientations. We see in Fig. 7 that capture wells are absent for these systems when both nuclei are spherical. Moreover, the capture well for the reaction ^{70}Zn+^{238}U is extremely shallow when shapes of ^{70}Zn and ^{238}U are correspondingly treated as spherical and deformed (see Fig. 6 in Ref. [27]). However, the deep capture pockets are clearly seen for these systems in the case of both deformed nuclei at orientation $\Theta_1 = 90^\circ$ and $\Theta_2 = 60^\circ$–90° in Fig 7. The deep capture pockets for these reactions at $\Theta_1 = 90^\circ$ and $\Theta_2 = 60^\circ$–90° are induced by the strong deformation of interacting nuclei. The depths of capture wells for these reactions are similar to the ones for the cold-fusion reaction ^{48}Ca+^{208}Pb or hot-fusion reactions with ^{48}Ca beam (see Figs. 2 and 4 in Ref. [27]). Thus the systems Zn+Th and Zn+U should be captured in the potential pocket at incoming orientations around $\Theta_1 = 90^\circ$ and $\Theta_2 = 60^\circ$–90°. The successful capture can lead to the reasonable probability of the SHE formation, because the shape of the nuclear system around the capture pocket at these orientations is compact. The nucleus-nucleus capture for the systems ^{64,70}Zn+^{232}Th and

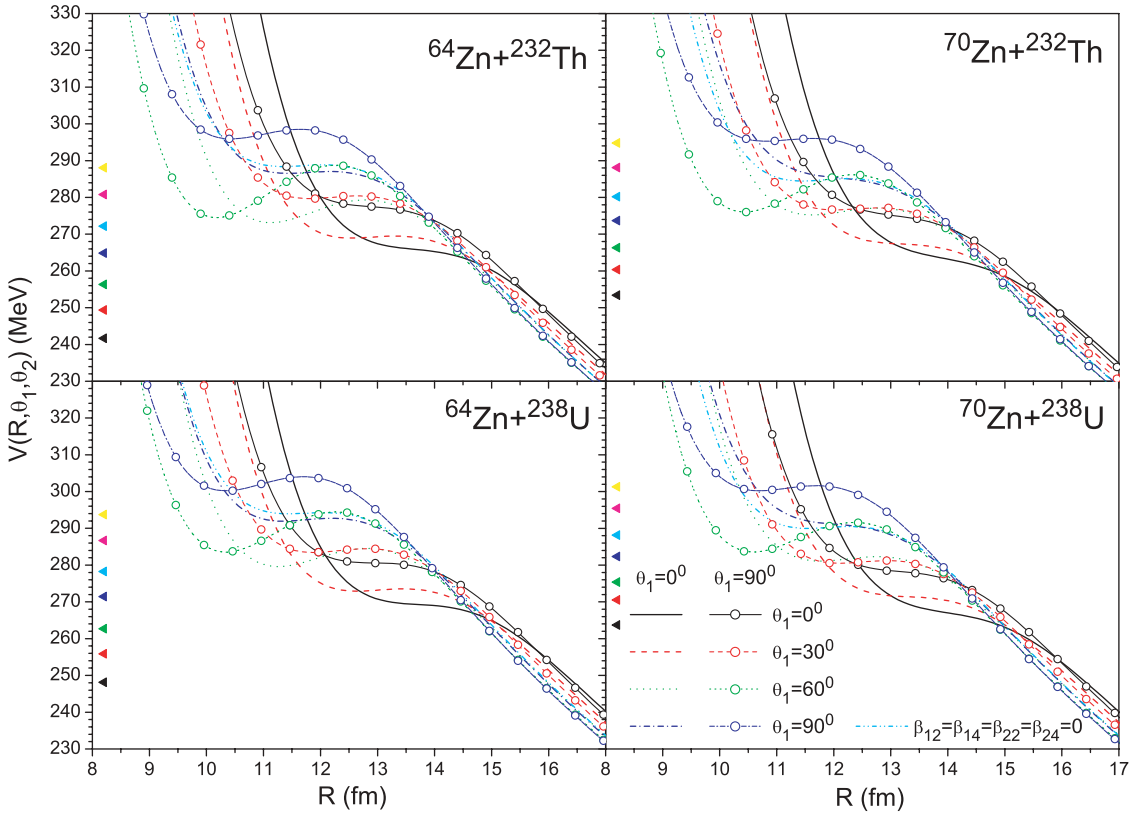

FIG. 7. (Color online) Nucleus-nucleus potentials for the systems ^{64,70}Zn+^{232}Th and ^{64,70}Zn+^{238}U for various orientations. The potential between the spherical nuclei ($\beta_{12} = \beta_{14} = \beta_{22} = \beta_{24} = 0$) for each system is also presented on each panel. The notations are the same as in Fig. 5. The ground-state reaction Q values and thresholds for the neutron emissions are evaluated by using experimental [53] and theoretical [44] binding energies.

^{64,70}Zn+^{238}U is induced by both quadrupole and hexadecapole deformations of nuclei in the entrance channel. The capture pocket of potentials for the systems ^{64}Zn+^{232}Th,^{238}U at $\Theta_1 = 90^\circ$ and $\Theta_2 = 60^\circ$ is deeper than the one for systems with ^{70}Zn.

It is interesting to know the nature of the deep capture pockets that occurred at the orientation around $\Theta_1 = 90^\circ$ and $\Theta_2 = 60^\circ$ for the Zn+Th,U potentials in Fig 7. We discuss the reason for this peculiarity of the interaction potential by drawing a picture with a realistic shape of the nuclei in the planes $X_1O_1Z_1$ and $X_2O_2Z_2$ (see Fig. 1 for the definition of the coordinate systems and corresponding planes). The shape of the system ^{64}Zn+^{238}U with values of deformation parameters from Table I at the plane $X_1O_1Z_2$ at orientation $\Theta_1 = 90^\circ$, $\Theta_2 = 60^\circ$, and $\Phi = 0^\circ$ at a distance between mass centers $R = 14$ fm is presented in Fig. 8. We see that the curvatures of nuclear surfaces at the closest points A and B are large around such orientation because of the influence of hexadecapole deformation of heavy nuclei. We point out here that the minimal values of the hexadecapole spherical harmonic function take place at $\vartheta \approx 49^\circ$ or $\vartheta \approx 131^\circ$, $Y_{40}(\vartheta)|_{\vartheta=49^\circ,131^\circ} \approx -0.36$. We see in Fig. 8 that the angle $BO_2Z_2' \approx 129^\circ$ is close to the minimum point of $Y_{40}(\vartheta)$ at $\vartheta \approx 131^\circ$. The nuclear part of the potential depends on the curvatures, therefore the capture well depth at $\Theta_1 = 90^\circ$ and $\Theta_2 = 60^\circ$ is larger than the one for $\Theta_1 = \Theta_2 = 90^\circ$ because of the smaller value of the ^{238}U surface curvatures around the equator.

We see in Fig. 8 that points A and B are located approximately 1 fm below the line connecting the mass centers of interacting nuclei O_1O_2. Line AB is not parallel to the

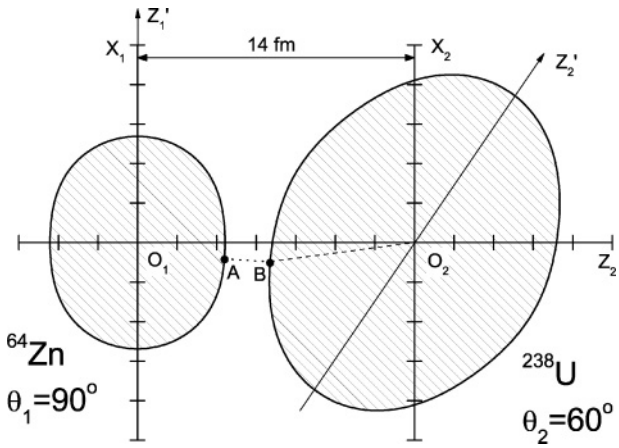

FIG. 8. Shape of ^{64}Zn+^{238}U system at orientation $\Theta_1 = 90^\circ$, $\Theta_2 = 60^\circ$, and $\Phi = 0^\circ$ at a 14 fm distance between mass centers. Dots A and B mark the closest points between nuclei ^{64}Zn and ^{238}U. O_1Z_1' and O_2Z_2' are the axial-symmetry axes of, respectively, ^{64}Zn and ^{238}U.

axis O_1Z_2. Therefore various approximations for the nuclear part of the nucleus-nucleus interaction which used only the distance between mass centers can lead to significant error for the potential between well-deformed nuclei.

The excitation energies of the compound-nuclei formed in reactions ^{64}Zn+^{232}Th,^{238}U and ^{70}Zn+^{232}Th,^{238}U at collision energies around the barrier at orientation $\Theta_1 = 90^\circ$ and $\Theta_2 = 60^\circ$ are close to the threshold for the $6n$ and $5n$ emissions, respectively. We point out that the collision energy close to the threshold for the $5n$ emission from the compound nucleus is successfully used in experiments with a ^{48}Ca beam [7,27]. Therefore the capture process and compound-nucleus excitations for reactions with ^{64,70}Zn and ^{48}Ca are similar. As a result, it is very hopeful that the experimental study of the reactions ^{64,70}Zn+^{232}Th and ^{64,70}Zn+^{238}U would lead to elements with 120 and 122 protons. It is very questionable to synthesize these elements in the cold-fusion reactions Sr,Zr+^{208}Pb because of the vanishing capture, as well as in the hot-fusion reactions ^{48}Ca+Fm,No because of problems with the target material. We see that the reactions ^{64,70}Zn+^{232}Th and ^{64,70}Zn+^{238}U give us a unique practical possibility for the formation of elements with 120 and 122 protons at energies around 274–288 and 282–294 MeV, respectively. (Note that a reaction with the Fe or Ni beam can be attractive from some points of view too; however, stable Fe or Ni isotopes are either spherical or weakly deformed in contrast to Zn isotopes. Therefore the deformation enhancement of the capture well depth is absent for reactions between Fe or Ni and heavy transuranium nuclei.) These collision energies for reactions leading to elements with 120 and 122 protons belong to the interval between the side-tip and side-side barriers discussed in the previous subsection.

The numbers of neutrons in the compound nucleus formed in reactions with ^{64}Zn are 176 and 180, correspondingly, while the ones for reactions with ^{70}Zn are, respectively, 182 and 186. These numbers are close to the neutron magic number 184. Note that numbers 184 for neutron and 120 for proton are predicted as magic in the framework of various theories (see. Ref. [66] and references therein). As a result, the compound nuclei formed in these reactions should be relatively stable. This peculiarity also supports the experimental study of the reactions ^{64,70}Zn+^{232}Th and ^{64,70}Zn+^{238}U.

D. Potential for ultraheavy systems

Attempts for synthesis of SHE are mostly related to the fusion reaction [7]. However, the multiparticle transfer between both very heavy nuclei can be considered as alternative pathway for SHE production. The multiparticle transfer in the reactions ^{238}U+^{238}U, ^{238}U+^{248}Cm, and Xe+^{248}Cm have been studied experimentally and theoretically [8–10,67,68].

We present the results for the nucleus-nucleus potentials for the system ^{238}U+^{238}U for various orientations in Fig. 9. There is no potential pocket typical for lighter systems, the potential is repulsive everywhere. This feature of potentials is a direct consequence of the tendency pointed out in Ref. [27] that the potential pocket vanishes with increasing size of the projectile and target for spherical and spherical-deformed systems. This feature is confirmed by the results presented in Figs. 4–7 and 9.

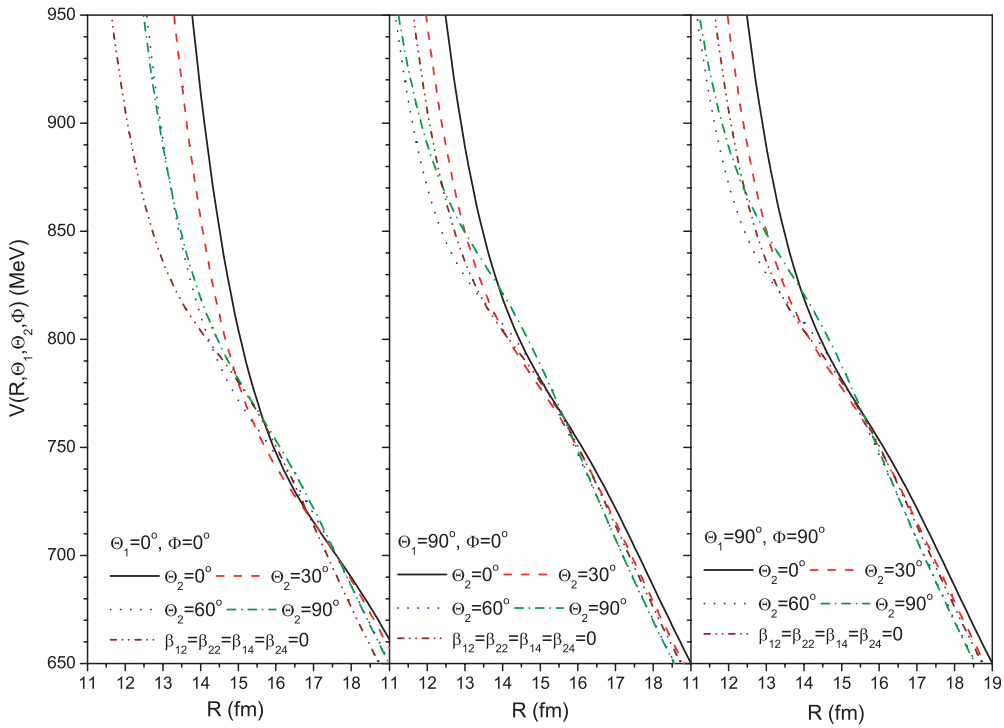

FIG. 9. (Color online) Nucleus-nucleus potentials for the system ^{238}U+^{238}U for various orientations. The potential between spherical nuclei ($\beta_{12} = \beta_{14} = \beta_{22} = \beta_{24} = 0$) for each system is also presented on each panel.

The influence of nuclear interaction on the total nucleus-nucleus potential appears as the variation of the slope of the lines in Fig. 9 at $R \approx 13$–17 fm. The position of the slope variation depends on the orientation of the colliding nuclei. The variation of the side-side potential at different angle Φ at the side-side orientation is several MeVs. This variation is relatively small in comparison with the value of the potential around the touching point.

The multiparticle transfer for the reaction ^{238}U+^{238}U is studied at the energy $E_{\text{c.m.}} = 892.5$ MeV with a thick target [8]. Therefore the nuclei are strongly overlapped at any orientation at this collision energy. The quasielastic transfer channels and damped collisions with the associated fission process give the main contribution to the reaction cross section [8]. The heaviest nucleus formed by multiparticle transfer in this reaction is ^{256}Fm [8].

The probability of multiparticle transfer between heavy nuclei is highest when the area of the surfaces belonging to incoming nuclei close to each other is the largest and the time of close contact of two nuclei is the longest. The nuclear part of the interaction between ions is proportional to the area of the surfaces, which strongly interact. Therefore orientations $\Theta_{1,2} \approx 60^\circ$–$90^\circ$ are related to the strongest nuclear interactions between colliding nuclei. The time of close contact of two nuclei is largest for the case of the lowest slope of the potential around a turning point. Analyzing results for potential at $\Theta_1 = 90^\circ$, $\Theta_2 = 60^\circ$–90°, and $\Phi = 0^\circ$ in the middle panel of Fig. 9, we conclude that the SHE production by massive transfer in the reaction ^{238}U+^{238}U should be the most effective at collision energies around 830–880 MeV.

Note that the nucleus-nucleus orientation $\Theta_1 = \Theta_2 = 90^\circ$ leads to the lowest values of Coulomb potential at large distances between ions, see Fig. 9. In contrast to this, the Coulomb potential evaluated at the orientation $\Theta_1 = \Theta_2 = 0^\circ$ is the highest.

V. CONCLUSIONS

We derive the expression for the Coulomb interaction of two deformed, arbitrarily oriented nuclei. The nuclear part of the nucleus-nucleus potential is obtained by numerical evaluation of the closest distance between surfaces of interacting nuclei and expressions for both the surface curvatures and the nucleus-nucleus potential between spherical nuclei. The potential evaluated in the framework of this approach agrees well with the one evaluated by direct numerical semimicroscopic calculation.

We show that the nucleus-nucleus potential depends strongly on both the values of deformation parameters and mutual orientation of nuclei. The more compact nucleus-nucleus shapes lead to a higher barrier height and deeper capture well. We point out here that the capture well properties determine the shape evolution of the nuclear system from the touching configuration of two nuclei to the compound nucleus. The large depth and width of the capture well are favorable to the successful capture of colliding nuclei and further formation of the compound nucleus.

The deformation of both nuclei and their mutual orientation strongly influence the barrier height and position. The range of barrier height variation induced by mutual orientation of heavy well-deformed nuclei is approximately 15–20 MeV. The range of barrier distance change is around 2.5 fm. Because of this, the deformation of nuclei and their mutual orientation during approach are extremely important for subbarrier and near-barrier heavy-ion fusion studies. Knowing the barrier heights, ground-state reaction Q value, neutron separation energies, and fission barrier, we can analyze the reaction mechanism and choose the optimal condition for the SHE production. We show that the experimental energies chosen for SHE formation in very asymmetric reactions are close to the side-side barrier height.

The leading deformation effect on the potential is related to the quadrupole deformation. However, the hexadecapole deformation of a heavy nucleus is also very important for the accurate evaluation of the barrier and especially the capture well. Due to considerable quadrupole deformations in both nuclei and noticeable hexadecapole deformations, reactions Zn+Th,U are very promising for the synthesis of very heavy nuclei.

The Bass potential [54] is often used to evaluate the barrier height between two nuclei leading to SHE. The spherical shape of both nuclei is considered for the Bass potential [54]. We see here that the barrier heights evaluated for spherical and two deformed nuclei are very different. The tip-tip or side-side barrier heights for very asymmetric heavy systems in Figs. 2, 4–7 are approximately 10 MeV lower or higher than the barrier heights for the same spherical nuclei. Therefore application of any potential evaluated for spherical nuclei [54, 57] to the case of well-deformed nuclei without taking into account surface curvature and deformation effects leads to an inadequate picture of the reaction mechanism.

ACKNOWLEDGMENT

The authors thanks V. I. Tretyak for useful remarks.

[1] M. Beckerman, Rep. Prog. Phys. **51**, 1047 (1988); M. Dasgupta, D. J. Hinde, N. Rowley, and A. M. Stefanini, Annu. Rev. Nucl. Part. Sci. **48**, 401 (1998); A. B. Balantekin and N. Takigawa, Rev. Mod. Phys. **70**, 77 (1998); L. F. Canto, P. R. S. Gomes, R. Donangelo, and M. S. Hussein, Phys. Rep. **424**, 1 (2006).

[2] C. Y. Wong, Phys. Rev. Lett. **31**, 766 (1973).

[3] J. O. Fernandez-Niello, C. H. Dasso, and S. Landowne, Comput. Phys. Commun. **54**, 409 (1989).

[4] C. H. Dasso, J. Fernandez-Niello, and S. Landowne, Phys. Rev. C **41**, 1014 (1990).

[5] T. Rumin, K. Hagino, and N. Takigawa, Phys. Rev. C **61**, 014605 (2000).

[6] V. Yu. Denisov and H. Ikezoe, Phys. Rev. C **72**, 064613 (2005).

[7] H. Hofmann and G. Münzenberg, Rev. Mod. Phys. **72**, 733 (2000); P. Armbruster, Annu. Rev. Nucl. Part. Sci. **50**, 411 (2000); Yu. Ts. Oganessian, Nucl. Phys. **A734**, 109 (2004); M. Gupta and T. W. Burrows, Nucl. Data Sheets **106**, 251 (2005);

Yu. Ts. Oganessian, Phys. At. Nucl. **69**, 932 (2006); S. Hofmann, D. Ackermann, S. Antalic, H. G. Burkhard, R. Dressler, F. P. Hessberger, B. Kindler, I. Kojouharov, P. Kuusiniemi, M. Leino, B. Lommel, R. Mann, G. Münzenberg, K. Nishio, A. G. Popeko, S. Saro, H. J. Schött, B. Streicher, B. Sulignano, J. Uusitalo, and A. V. Yeremin, J. Nucl. Radiochem. Sci. **7**, R25 (2006); Yu. Ts. Oganessian, V. K. Utyonkov, Yu. V. Lobanov, F. Sh. Abdullin, A. N. Polyakov, R. N. Sagaidak, I. V. Shirokovsky, Yu. S. Tsyganov, A. A. Voinov, G. G. Gulbekian, S. L. Bogomolov, B. N. Gikal, A. N. Mezentsev, S. Iliev, V. G. Subbotin, A. M. Sukhov, K. Subotic, V. I. Zagrebaev, G. K. Vostokin, M. G. Itkis, K. J. Moody, J. B. Patin, D. A. Shaughnessy, M. A. Stoyer, N. J. Stoyer, P. A. Wilk, J. M. Kenneally, J. H. Landrum, J. F. Wild, and R. W. Lougheed, Phys. Rev. C **74**, 044602 (2006).

[8] M. Schädel, J. V. Kratz, H. Ahrens, W. Brüchle, G. Franz, H. Gäggeler, I. Warnecke, G. Wirth, G. Herrmann, N. Trautmann, and M. Weis, Phys. Rev. Lett. **41**, 469 (1978); H. Gäggeler, N. Trautmann, W. Brüchle, G. Herrmann, J. V. Kratz, P. Peuser, M. Schädel, G. Tittel, G. Wirth, H. Ahrens, H. Folger, G. Franz, K. Sümmerer, and M. Zendel, *ibid.* **45**, 1824 (1980).

[9] M. Schädel, W. Brüchle, H. Gäggeler, J. V. Kratz, K. Sümmerer, G. Wirth, G. Herrmann, R. Stakemann, G. Tittel, N. Trautmann, J. M. Nitschke, E. K. Hulet, R. W. Lougheed, R. L. Hahn, and R. L. Ferguson, Phys. Rev. Lett. **48**, 852 (1982).

[10] R. B. Welch, K. J. Moody, K. E. Gregorich, D. Lee, and G. T. Seaborg, Phys. Rev. C **35**, 204 (1987).

[11] D. Lee, H. von Gunten, B. Jacak, M. Nurmia, Y. F. Liu, C. Luo, G. T. Seaborg, and D. C. Hoffman, Phys. Rev. C **25**, 286 (1982); Yu. A. Lazarev, Yu. V. Lobanov, Yu. Ts. Oganessian, V. K. Utyonkov, F. Sh. Abdullin, G. V. Buklanov, B. N. Gikal, S. Iliev, A. N. Mezentsev, A. N. Polyakov, I. M. Sedykh, I. V. Shirokovsky, V. G. Subbotin, A. M. Sukhov, Yu. S. Tsyganov, V. E. Zhuchko, R. W. Lougheed, K. J. Moody, J. F. Wild, E. K. Hulet, and J. H. McQuaid, Phys. Rev. Lett. **73**, 624 (1994); A. Türler, R. Dressler, B. Eichler, H. W. Gäggeler, D. T. Jost, M. Schädel, W. Brüchle, K. E. Gregorich, N. Trautmann, and S. Taut, Phys. Rev. C **57**, 1648 (1998); M. G. Itkis, N. A. Kondratiev, E. M. Kozulin, Yu. Ts. Oganessian, I. V. Pokrovsky, E. V. Prokhorova, and A. Ya. Rusanov, *ibid.* **59**, 3172 (1999).

[12] M. R. Lane, K. E. Gregorich, D. M. Lee, M. F. Mohar, M. Hsu, C. D. Kacher, B. Kadkhodayan, M. P. Neu, N. J. Stoyer, E. R. Sylwester, J. C. Yang, and D. C. Hoffman, Phys. Rev. C **53**, 2893 (1996).

[13] R. N. Sagaidak, V. I. Chepigin, A. P. Kabachenko, J. Rohac, Yu. Ts. Oganessian, A. G. Popeko, A. V. Eremin, A. D'Arrigo, G. Fazio, G. Gardina, M. Herman, R. Ruggeri, and R. Sturiale, J. Phys. G: Nucl. Part. Phys. **24**, 611 (1998).

[14] R. Dressler, B. Eichler, D. T. Jost, D. Piguet, A. Türler, Ch. Düllmann, R. Eichler, H. W. Gäggeler, M. Gärtner, M. Schädel, S. Taut, and A. B. Yakushev, Phys. Rev. C **59**, 3433 (1999); Y. Nagame, M. Asai, H. Haba, S. Goto, K. Tsukada, I. Nishinaka, K. Nishio, S. Ichikawa, A. Toyoshima, K. Akiyama, H. Nakahara, M. Sakama, M. Schädel, J. V. Kratz, H. W. Gäggeler, and A. Türler, J. Nucl. Radiochem. Sci. **3**, 85 (2002); D. Trubert, C. Le Naour, F. Monroy Guzman, M. Hussonnois, L. Brillard, J. F. Le Du, O. Constantinescu, J. Gasparro, V. Barci, B. Weiss, and G. Ardisson, Radiochim. Acta **90**, 127 (2002).

[15] Yu. A. Lazarev, Yu. V. Lobanov, Yu. Ts. Oganessian, V. K. Utyonkov, F. Sh. Abdullin, A. N. Polyakov, J. Rigol, I. V. Shirokovsky, Yu. S. Tsyganov, S. Iliev, V. G. Subbotin, A. M. Sukhov, G. V. Buklanov, A. N. Mezentsev, K. Subotic, K. J. Moody, N. J. Stoyer, J. F. Wild, and R. W. Lougheed, Phys. Rev. C **62**, 064307 (2000).

[16] P. A. Wilk, K. E. Gregorich, A. Türler, C. A. Laue, R. Eichler, V. Ninov, J. L. Adams, U. W. Kirbach, M. R. Lane, D. M. Lee, J. B. Patin, D. A. Shaughnessy, D. A. Strellis, H. Nitsche, and D. C. Hoffman, Phys. Rev. Lett. **85**, 2697 (2000).

[17] Z. G. Gan, Z. Qin, H. M. Fan, X. G. Lei, Y. B. Xu, J. J. He, H. Y. Liu, X. L. Wu, J. S. Guo, X. H. Zhou, S. G. Yuan, and G. M. Jin, Eur. Phys. J. A **10**, 21 (2001).

[18] A. Türler, Ch. E. Düllmann, H. W. Gäggeler, U. W. Kirbach, A. B. Yakushev, M. Schädel, W. Brüchle, R. Dressler, K. Eberhardt, B. Eichler, R. Eichler, T. N. Ginter, F. Glaus, K. E. Gregorich, D. C. Hoffman, E. Jäger, D. T. Jost, D. M. Lee, H. Nitsche, J. B. Patin, V. Pershina, D. Piguet, Z. Qin, B. Schausten, E. Schimpf, H. J. Schött, S. Soverna, R. Sudowe, P. Thorle, S. N. Timokhin, N. Trautmann, A. Vahle, G. Wirth, and P. M. Zielinski, Eur. Phys. J. A **17**, 505 (2003); J. Dvorak, W. Brüchle, M. Chelnokov, R. Dressler, Ch. E. Düllmann, K. Eberhardt, V. Gorshkov, E. Jäger, R. Krücken, A. Kuznetsov, Y. Nagame, F. Nebel, Z. Novackova, Z. Qin, M. Schädel, B. Schausten, E. Schimpf, A. Semchenkov, P. Thörle, A. Türler, M. Wegrzecki, B. Wierczinski, A. Yakushev, and A. Yeremin, Phys. Rev. Lett. **97**, 242501 (2006).

[19] Z. G. Gan, J. S. Guo, X. L. Wu, Z. Qin, H. M. Fan, X. G. Lei, H. Y. Liu, B. Guo, H. G. Xu, R. F. Chen, C. F. Dong, F. M. Zhang, H. L. Wang, C. Y. Xie, Z. Q. Feng, Y. Zhen, L. T. Song, P. Luo, H. S. Xu, X. H. Zhou, G. M. Jin, and Z. Ren, Eur. Phys. J. A **20**, 385 (2004).

[20] A. Türler, J. Nucl. Radiochem. Sci. **5**, R19 (2004).

[21] S. L. Shapiro, S. A. Teukolsky, *Black Holes, White Dwarfs, and Neutron Stars* (Wiley, New York, 1983).

[22] H. A. Bethe, Rev. Mod. Phys. **62**, 801 (1990).

[23] S. E. Woosley, A. Heger, and T. A. Weaver, Rev. Mod. Phys. **74**, 1015 (2002).

[24] G. R. Satchler, *Direct Nuclear Reactions* (Oxford University, Oxford, 1983).

[25] K. Alder and A. Winther, Nucl. Phys. **A132**, 1 (1969).

[26] V. Yu. Denisov, Phys. Lett. **B526**, 315 (2002).

[27] V. Yu. Denisov and W. Nörenberg, Eur. Phys. J. A **15**, 375 (2002); V. Yu. Denisov, *ibid.* **25**, Supplement 1, 619 (2005).

[28] P. Möller and A. Iwamoto, Nucl. Phys. **A575**, 381 (1994); A. Iwamoto, P. Möller, J. R. Nix, and H. Sagawa, Nucl. Phys. **A596**, 329 (1996).

[29] T. Ichikawa, A. Iwamoto, P. Möller, and A. J. Sierk, Phys. Rev. C **71**, 044608 (2005).

[30] L. C. Chamon, B. V. Carlson, L. R. Gasques, D. Pereira, C. De Conti, M. A. G. Alvarez, M. S. Hussein, M. A. Candido Ribeiro, E. S. Rossi, and C. P. Silva, Phys. Rev. C **66**, 014610 (2002); L. C. Chamon, G. P. A. Nobre, D. Pereira, E. S. Rossi, C. P. Silva, L. R. Gasques, and B. V. Carlson, *ibid.* **70**, 014604 (2004).

[31] M. Ismail, W. M. Seif, M. M. Osman, H. El-Gebaly, and N. M. Hassan, Phys. Rev. C **72**, 064616 (2005).

[32] A. J. Baltz and B. F. Bayman, Phys. Rev. C **26**, 1969 (1982); B. F. Bayman, *ibid.* **34**, 1346 (1986).

[33] M. Seiwert, W. Greiner, V. Oberacker, and M. J. Rhoades-Brown, Phys. Rev. C **29**, 477 (1984).

[34] S. Misicu and W. Greiner, Phys. Rev. C **66**, 044606 (2002).

[35] R. A. Broglia, C. H. Dasso, H. Esbensen, and A. Winther, Nucl. Phys. **A349**, 496 (1980).

[36] J. O. Newton, R. D. Butt, M. Dasgupta, D. J. Hinde, I. I. Gontchar, C. R. Morton, and K. Hagino, Phys. Rev. C **70**, 024605 (2004).
[37] V. Yu. Denisov, AIP Conf. Proc. **704**, 92 (2004); Acta Phys. Hung. A **19**, 121 (2004).
[38] J. Blocki, J. Randrup, W. J. Swiatecki, and C. F. Tsang, Ann. Phys. (NY) **105**, 427 (1977).
[39] R. K. Gupta, N. Singh, and M. Manhas, Phys. Rev. C **70**, 034608 (2004); M. Manhas and R. K. Gupta, *ibid*. **72**, 024606 (2005); R. K. Gupta, M. Manhas, and W. Greiner, *ibid*. **73**, 054307 (2006).
[40] W. Nörenberg, in *Proceedings of Workshop on Heavy-Ion Fusion: Exploring the Variety of Nuclear Properties, Padova, 1994*, edited by A. M. Stefanini *et al.* (World Scientific, Singapore, 1994), p. 248.
[41] V. Yu. Denisov and N. A. Pilipenko, in *Proceedings of the International Conference on Current Problems in Nuclear Physics and Atomic Energy, May 29–June 2, 2006, Kiev* (Institute for Nuclear Research, Kiev, 2007), p. 115.
[42] D. A. Varshalovich, A. N. Moskalev, and V. K. Khersonskii, *Kvantovaya Teoriya Uglovogo Momenta* (Izdatelstvo Nauka, Leningrad, 1975) [English translation: *Quantum Theory of Angular Momentum* (World Scientific, Singapore, 1988)].
[43] B. C. Carlson and G. S. Rushbrooke, Proc. Cambridge Philos. Soc. **46**, 626 (1950).
[44] P. Möller, J. R. Nix, W. D. Myers, and W. J. Swiatecki, At. Data Nucl. Data Tables **59**, 195 (1995).
[45] S. Goriely, F. Tondeur, and J. M. Pearson, At. Data Nucl. Data Tables **77**, 311 (2001).
[46] G. A. Lalazissis, S. Raman, and P. Ring, At. Data Nucl. Data Tables **71**, 1 (1999).
[47] Q. Zhi and Z. Ren, J. Phys. G: Nucl. Part. Phys. **32**, 375 (2006).
[48] G. R. Satchler and W. G. Love, Phys. Rep. **55**, 183 (1979).
[49] V. Yu. Denisov and V. A. Nesterov, Phys. At. Nucl. **69**, 1472 (2006); Ukr. Phys. J. **51**, 440 (2006); in *Proceedings of the International Conference on Current Problems in Nuclear Physics and Atomic Energy, May 29–June 2, 2006, Kiev* (Institute for Nuclear Research, Kiev, 2007), p. 108.
[50] R. A. Broglia, C. H. Dasso, and A. Winther, in *Proceedings of the International School of Physics "Enrico Fermi," Nuclear Structure and Heavy-Ion Collisions, Varenna, July 1979* (North-Holland, Amsterdam, 1981), p. 327.
[51] G. A. Korn and T. M. Korn, *Mathematical Handbook for Scientist and Engineers* (McGraw-Hill, New York, 1961).
[52] S. Raman, C. W. Nestor, and P. Tikkanen, At. Data Nucl. Data Tables **78**, 1 (2001).
[53] G. Audi, O. Bersillon, J. Blachot, and A. H. Wapstra, Nucl. Phys. **A729**, 3 (2003).
[54] R. Bass, *Nuclear Reactions with Heavy Ions* (Springer-Verlag, Berlin, 1980).
[55] W. D. Myers and W. J. Swiatecki, Phys. Rev. C **62**, 044610 (2000).
[56] H. J. Krappe, J. R. Nix, and A. J. Sierk, Phys. Rev. C **20**, 992 (1979).
[57] A. Winther, Nucl. Phys. **A594**, 203 (1995).
[58] V. Yu. Denisov and S. Hofmann, Phys. Rev. C **61**, 034606 (2000).
[59] S. Mitsuoka, H. Ikezoe, K. Nishio, and J. Lu, Phys. Rev. C **62**, 054603 (2000); K. Nishio, H. Ikezoe, S. Mitsuoka, and J. Lu, *ibid.* **62**, 014602 (2000); H. Ikezoe, S. Mitsuoka, K. Nishio, K. Satou, and I. Nishinaka, J. Nucl. Radiochem. Sci. **3**, 39 (2002).
[60] D. J. Hinde, M. Dasgupta, J. R. Leigh, J. P. Lestone, J. C. Mein, C. R. Morton, J. O. Newton, and H. Timmers, Phys. Rev. Lett. **74**, 1295 (1995).
[61] K. Nishio, H. Ikezoe, Y. Nagame, M. Asai, K. Tsukada, S. Mitsuoka, K. Tsuruta, K. Satou, C. J. Lin, and T. Ohsawa, Phys. Rev. Lett. **93**, 162701 (2004).
[62] K. Nishio, S. Hofmann, F. P. Hessberger, D. Ackermann, S. Antalic, V. F. Comas, Z. Gan, S. Heinz, J. A. Heredia, H. Ikezoe, J. Khuyagbaatar, B. Kindler, I. Kojouharov, P. Kuusiniemi, B. Lommel, R. Mann1, M. Mazzocco, S. Mitsuoka, Y. Nagame, T. Ohtsuki, A. G. Popeko, S. Saro, H. J. Schött, B. Sulignano, A. Svirikhin, K. Tsukada, K. Tsuruta, and A. V. Yeremin, Eur. Phys. J. A **29**, 281 (2006).
[63] I. Muntian, Z. Patyk, and A. Sobiczewski, Acta Phys. Pol. B **34**, 2141 (2003).
[64] R. Smolanczuk, J. Skalski, and A. Sobiczewski, Phys. Rev. C **52**, 1871 (1995).
[65] Yu. Ts. Oganessian, V. K. Utyonkov, Yu. V. Lobanov, F. Sh. Abdullin, A. N. Polyakov, R. N. Sagaidak, I. V. Shirokovsky, Yu. S. Tsyganov, A. A. Voinov, G. G. Gulbekian, S. L. Bogomolov, B. N. Gikal, A. N. Mezentsev, S. Iliev, V. G. Subbotin, A. M. Sukhov, K. Subotic, V. I. Zagrebaev, G. K. Vostokin, M. G. Itkis, K. J. Moody, J. B. Patin, D. A. Shaughnessy, M. A. Stoyer, N. J. Stoyer, P. A. Wilk, J. M. Kenneally, J. H. Landrum, J. F. Wild, and R. W. Lougheed, Phys. Rev. C **74**, 044602 (2006).
[66] V. Yu. Denisov, Phys. At. Nucl. **68**, 1133 (2005); **70**, 244 (2007).
[67] C. Riedel and W. Nörenberg, Z. Phys. A **290**, 385 (1979).
[68] W. Greiner and V. Zagrebaev, J. Nucl. Radiochem. Sci. **7**, R1 (2006).